

An aged immune system drives senescence and ageing of solid organs

<https://doi.org/10.1038/s41586-021-03547-7>

Received: 4 March 2019

Accepted: 13 April 2021

Published online: 12 May 2021

 Check for updates

Matthew J. Yousefzadeh^{1,2,14}, Rafael R. Flores^{1,2,14}, Yi Zhu³, Zoe C. Schmiechen⁴, Robert W. Brooks⁵, Christy E. Trussoni⁶, Yuxiang Cui⁷, Luise Angelini^{1,2}, Kyoo-A Lee^{1,2}, Sara J. McGowan^{1,2}, Adam L. Burrack⁴, Dong Wang⁸, Qing Dong⁸, Aiping Lu⁹, Tokio Sano⁵, Ryan D. O'Kelly^{1,2}, Collin A. McGuckian^{1,2}, Jonathan I. Kato⁵, Michael P. Bank⁵, Erin A. Wade⁵, Smitha P. S. Pillai¹⁰, Jenna Klug¹¹, Warren C. Ladiges¹¹, Christin E. Burd¹², Sara E. Lewis¹³, Nicholas F. LaRusso⁶, Nam V. Vo⁸, Yinsheng Wang⁷, Eric E. Kelley¹³, Johnny Huard⁹, Ingunn M. Stromnes⁴, Paul D. Robbins^{1,2}✉ & Laura J. Niedernhofer^{1,2}✉

Ageing of the immune system, or immunosenescence, contributes to the morbidity and mortality of the elderly^{1,2}. To define the contribution of immune system ageing to organism ageing, here we selectively deleted *Ercc1*, which encodes a crucial DNA repair protein^{3,4}, in mouse haematopoietic cells to increase the burden of endogenous DNA damage and thereby senescence^{5–7} in the immune system only. We show that *Vav-iCre^{+/-};Ercc1^{-/-}* mice were healthy into adulthood, then displayed premature onset of immunosenescence characterized by attrition and senescence of specific immune cell populations and impaired immune function, similar to changes that occur during ageing in wild-type mice^{8–10}. Notably, non-lymphoid organs also showed increased senescence and damage, which suggests that senescent, aged immune cells can promote systemic ageing. The transplantation of splenocytes from *Vav-iCre^{+/-};Ercc1^{-/-}* or aged wild-type mice into young mice induced senescence *in trans*, whereas the transplantation of young immune cells attenuated senescence. The treatment of *Vav-iCre^{+/-};Ercc1^{-/-}* mice with rapamycin reduced markers of senescence in immune cells and improved immune function^{11,12}. These data demonstrate that an aged, senescent immune system has a causal role in driving systemic ageing and therefore represents a key therapeutic target to extend healthy ageing.

Old age is the greatest risk factor, by orders of magnitude, for most chronic diseases¹. Diseases cluster in individuals so curing one disease will not affect the fraction of healthy elderly². This led to the argument for therapeutically targeting fundamental ageing processes to compress the period of morbidity in old age¹³. Proof of concept comes from a new class of drugs known as senolytics that selectively kill senescent cells⁶. Senescence is a tumour-suppressor mechanism that is activated in response to stress and results in cell cycle arrest and a secretory phenotype that is pro-inflammatory and tissue damaging¹⁴. Senescent cells are known to be key drivers of ageing, and senolytics are able to delay or attenuate numerous age-related diseases, suppress frailty and extend healthy ageing^{5–7}. It is clear that a single senolytic will not kill all senescent cells¹⁵. Therefore, which senescent cell types drive ageing most potently, and therefore are the most important to target therapeutically, remains a crucial question.

During ageing, the immune system loses its ability to mount an effective response against pathogens and cancer cells. This decline in immune function is termed immunosenescence and is characterized by changes in the naive:memory T cell ratio, CD4:CD8 ratio, impaired calcium-mediated signalling and thymic atrophy¹⁶. In addition, many immune cell types senesce with ageing, expressing increased levels of *p16^{INK4a}* (also known as *CDKN2A*) and *p21^{CIP1}* (*CDKN1A*) and a senescence-associated secretory phenotype (SASP)^{17–19}. These age-dependent changes limit the effectiveness of vaccinations, increase disease susceptibility, and contribute to mortality in older adults¹⁶. However, the contribution of the aged immune system to systemic ageing, independent of increasing susceptibility to infection and cancer, is poorly understood.

Reducing expression of the endonuclease ERCC1–XPF impairs the repair of DNA damage and accelerates accumulation of endogenous oxidative lesions and senescent cells in several tissues of mice^{3,4}. This

¹Institute on the Biology of Aging and Metabolism, University of Minnesota, Minneapolis, MN, USA. ²Department of Biochemistry, Molecular Biology and Biophysics, University of Minnesota, Minneapolis, MN, USA. ³Robert and Arlene Kogod Center on Aging, Mayo Clinic, Rochester, MN, USA. ⁴Center for Immunology, University of Minnesota Medical School, Minneapolis, MN, USA. ⁵Department of Molecular Medicine, The Scripps Research Institute, Jupiter, FL, USA. ⁶Division of Gastroenterology, Center for Cell Signaling in Gastroenterology, Mayo Clinic, Rochester, MN, USA. ⁷Department of Chemistry, University of California Riverside, Riverside, CA, USA. ⁸Department of Orthopaedic Surgery, University of Pittsburgh, Pittsburgh, PA, USA. ⁹Department of Orthopaedic Surgery, McGovern Medical School, University of Texas Health Science Center at Houston, Houston, TX, USA. ¹⁰Fred Hutchinson Cancer Research Center, Seattle, WA, USA. ¹¹Department of Comparative Medicine, University of Washington, Seattle, WA, USA. ¹²Departments of Molecular Genetics and Cancer Biology and Genetics, The Ohio State University, Columbus, OH, USA. ¹³Department of Physiology & Pharmacology, West Virginia University, Morgantown, WV, USA. ¹⁴These authors contributed equally: Matthew J. Yousefzadeh, Rafael R. Flores. ✉e-mail: probbins@umn.edu; lniedern@umn.edu

causes premature onset of morbidities and histopathology associated with old age in mice and humans^{20–24}. Thus, by removing this DNA repair enzyme, ageing is accelerated owing to normal physiological processes. Here, we used a floxed allele of *Ercc1* to determine the effect of the aged immune system on other tissues. The HS21/45 promoter of the mouse *Vav1* proto-oncogene was used to drive the expression of a codon-improved Cre recombinase²⁵ to delete *Ercc1* in haematopoietic cells, and the effect on the immune compartment and peripheral organs was evaluated.

Loss of immune cells

Vav-iCre^{+/+};Ercc1^{fl/fl} mice were bred and shown to have *Ercc1* knocked out in lymphoid organs but not in other tissues (Extended Data Fig. 1a, b). The C terminus of ERCC1, which was floxed, is essential for binding and stabilizing XPF (which is encoded by *Ercc4*) in vivo^{24,26}. Thus, the endonuclease ERCC1–XPF holoenzyme is absent in the immune compartment. *Vav-iCre^{+/+};Ercc1^{fl/fl}* mice were born with Mendelian frequency and showed no physical differences from littermates into adulthood (Extended Data Fig. 2). γ H2AX, a marker of genotoxic stress, was increased in splenic tissue from 8–10-month-old *Vav-iCre^{+/+};Ercc1^{fl/fl}* mice compared to controls, as were levels of the oxidative DNA lesion 8-oxo-guanine (Fig. 1a), consistent with a deficiency in the DNA repair machinery. Despite an increase in oxidative stress in the spleen and bone marrow of the *Vav-iCre^{+/+};Ercc1^{fl/fl}* mice (Extended Data Fig. 1c–i), other oxidative DNA lesions, cyclopurines, were not increased in splenic tissue from *Vav-iCre^{+/+};Ercc1^{fl/fl}* mice (Extended Data Fig. 1j). One explanation is that these lesions or a threshold of genotoxic stress kills immune cells, as reported for the nervous system⁴. Indeed, the *Vav-iCre^{+/+};Ercc1^{fl/fl}* mice developed a progressive peripheral leukopenia (Fig. 1b). The white blood cell count was not affected in younger mice, which indicates a degenerative rather than developmental process. A complete blood count revealed leukopenia was driven by a reduction of lymphocytes (Extended Data Table 1).

Flow cytometry of peripheral blood cells revealed that the fraction of T cells, but not B cells, was significantly reduced in *Vav-iCre^{+/+};Ercc1^{fl/fl}* mice compared to littermates at 4–5 months old (Fig. 1c). In older mutant mice, the fraction of T cells was reduced in the spleen and B cells were reduced in the bone marrow of *Vav-iCre^{+/+};Ercc1^{fl/fl}* mice relative to wild-type controls (Fig. 1d, e). This was confirmed by measuring the absolute numbers of splenocytes, B cells (B220⁺CD19⁺) and T cells (CD4⁺ and CD8⁺), which were all significantly reduced in *Vav-iCre;Ercc1^{fl/fl}* mice compared to controls (Extended Data Fig. 1k, l). By contrast, lymphocyte counts were stable during ageing in wild-type mice (Extended Data Fig. 1m, n).

There was a shift towards increased memory T cells (CD44⁺) (Fig. 1f) in the spleen of *Vav-iCre^{+/+};Ercc1^{fl/fl}* mice, similar to normal ageing¹⁶. PD-1, a marker of T cell activation and exhaustion²⁷, was increased in CD4⁺ cells from *Vav-iCre^{+/+};Ercc1^{fl/fl}* mouse spleen compared to controls (Fig. 1f). The caspase inhibitor and marker of apoptosis VAD-FMK was not significantly increased in splenic CD4⁺ and CD8⁺ cells from *Vav-iCre^{+/+};Ercc1^{fl/fl}* mice (Fig. 1f, Extended Data Fig. 1o). By 5 months of age, when DNA lesions were measured, mutant mice had significantly reduced numbers of immune cells in several compartments, and cell numbers continued to decline as the mice aged (Fig. 1b, Extended Data Table 1). Consistent with this, at 8–10 months of age, *Vav-iCre^{+/+};Ercc1^{fl/fl}* mice had reduced splenic and thymic weights (Fig. 1g, Extended Data Fig. 1p). Histopathological analysis of lymphoid tissues revealed loss of splenic germinal centres in *Vav-iCre^{+/+};Ercc1^{fl/fl}* mice as well as lymph node atrophy (Extended Data Fig. 1q). These data indicate that *Ercc1* deletion in haematopoietic cells causes an accelerated degenerative process in the immune system, similar, but not identical to what occurs with normal ageing in mice⁸. It also establishes that immune cells are vulnerable to endogenous DNA damage, which can cause cell death.

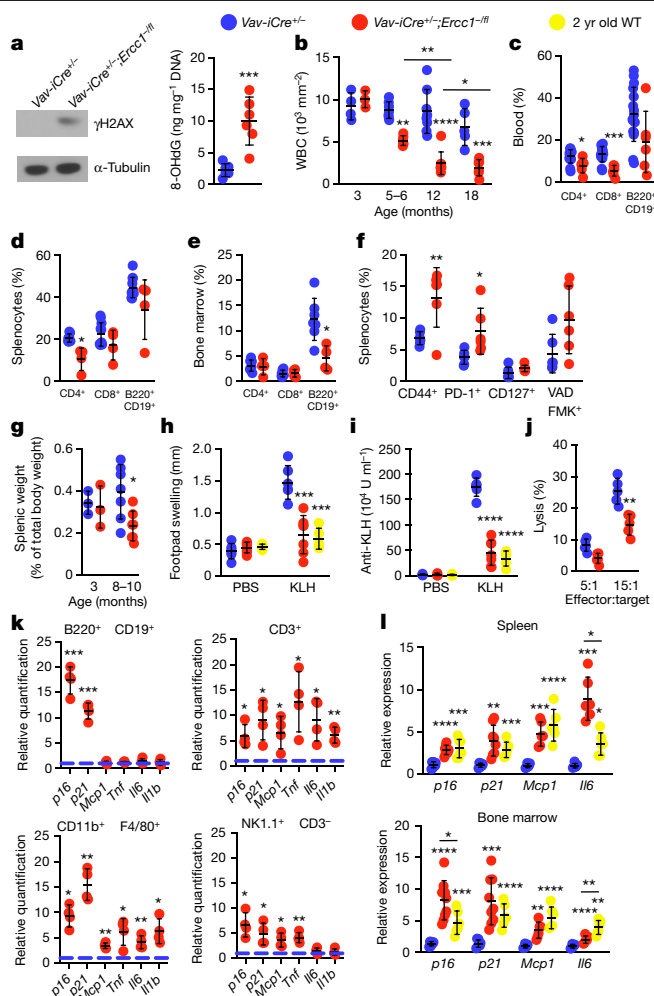


Fig. 1 | Deletion of *Ercc1* in haematopoietic cells causes accelerated ageing of the immune system. **a**, Immunoblot detection of γ H2AX in splenic lysates from 9-month-old mice. Levels of 8-oxo-guanine (8-OHdG) in spleens from 8–10-month-old mice ($n = 6$ mice per group). WT, wild type. **b**, Peripheral white blood cell (WBC) counts of *Vav-iCre^{+/+}* and *Vav-iCre^{+/+};Ercc1^{fl/fl}* mice ($n = 4, 7, 8$ and 5 *Vav-iCre^{+/+}*; $n = 3, 6, 8$ and 6 *Vav-iCre^{+/+};Ercc1^{fl/fl}*, at 3, 5–6, 12 and 18 months, respectively). **c**, Flow cytometric quantification of peripheral blood B and T cells in 4–5-month-old mice ($n = 15–16$ *Vav-iCre^{+/+}*; $n = 6$ *Vav-iCre^{+/+};Ercc1^{fl/fl}*) (see Supplementary Table 3 for sample size details). **d**, e, Splenic (d) and bone marrow (e) lymphocyte populations in 8–10-month-old mice ($n = 8–11/7$ *Vav-iCre^{+/+};Ercc1^{fl/fl}*; $n = 4/4$ *Vav-iCre^{+/+}* mice, for spleen/bone marrow). **f**, Analysis of CD4⁺ splenocytes from 8–10-month-old mice for memory (CD44⁺CD127⁺), exhaustion (PD-1⁺) and apoptosis (VAD-FMK⁺) markers ($n = 6$ mice per group). **g**, Splenic weights normalized to body weight ($n = 3$ at 3 months; $n = 7$ at 8–10 months). **h**, KLH delayed-type hypersensitivity data after sensitization of 5-month-old *Vav-iCre* or ≥ 24 -month-old wild-type mice. Footpad swelling at 48 h after challenge ($n = 6$ *Vav-iCre^{+/+}*; $n = 7$ *Vav-iCre^{+/+};Ercc1^{fl/fl}*; $n = 5$ WT). **i**, KLH antibodies measured by ELISA one month after challenge ($n = 3/6$ *Vav-iCre^{+/+}*; $n = 3/7$ *Vav-iCre^{+/+};Ercc1^{fl/fl}*; $n = 3/5$ 2-year-old wild-type challenged with PBS/KLH). **j**, Cytotoxicity of splenic natural killer cells from 8–12-month-old *Vav-iCre* mice ($n = 5$ mice per group). **k**, Senescence marker expression in flow-sorted cell populations from spleens (T, natural killer cells) and bone marrow (B cells, macrophages) of 5-month-old *Vav-iCre* mice ($n = 4$ mice per group). Expression is normalized to age-matched *Vav-iCre^{+/+}* controls (blue-dashed line). **l**, Senescence marker expression in splenic tissue (top) and bone marrow (bottom) from 8–11-month-old *Vav-iCre* and old wild-type mice ($n = 3–9$ *Vav-iCre^{+/+}*; $n = 6–9$ *Vav-iCre^{+/+};Ercc1^{fl/fl}*; $n = 4–7$ two-year-old WT, depending on the gene). Data are mean \pm s.d. * $P < 0.05$, ** $P < 0.01$, *** $P < 0.001$, **** $P < 0.0001$, unpaired two-tailed Student's *t*-test (**a**, **c–g**, **j**, **k**), one-way ANOVA (**h**, **i**) or two-way ANOVA (**b**) with Tukey's test.

Impaired immune function

To determine whether immune function is affected in *Vav-iCre^{+/+};Ercc1^{-/-}* mice, a delayed-type hypersensitivity (DTH) assay was performed. Five-month-old mutant mice and littermates, plus old wild-type mice, were immunized with keyhole limpet hemocyanin (KLH) then challenged 2 weeks later by the injection of antigen or vehicle into the footpad. Footpad swelling was reduced in *Vav-iCre^{+/+};Ercc1^{-/-}* and aged wild-type mice compared to young, wild-type mice (Fig. 1h, Extended Data Fig. 3a, b). Serum levels of anti-KLH antibodies were reduced in *Vav-iCre^{+/+};Ercc1^{-/-}* and aged wild-type mice (Fig. 1i, Extended Data Fig. 3c). This demonstrates that both cellular and humoral immune function were compromised in adult *Vav-iCre^{+/+};Ercc1^{-/-}* mice. Notably, two-month-old *Vav-iCre^{+/+};Ercc1^{-/-}* mice had a normal DTH response (Extended Data Fig. 3d), confirming that *Vav-iCre^{+/+};Ercc1^{-/-}* phenotypes are degenerative, analogous to ageing. Natural killer cell-mediated cytotoxicity, a biomarker of healthy immune ageing⁹, was impaired in *Vav-iCre^{+/+};Ercc1^{-/-}* mice (Fig. 1j). These data reveal innate and adaptive immune functions are impaired in *Vav-iCre^{+/+};Ercc1^{-/-}* mice.

Immune cell senescence

Senescence affects immune cell differentiation and function¹⁸. Immune cell populations were therefore isolated from lymphoid tissues collected from 5-month-old *Vav-iCre^{+/+};Ercc1^{-/-}* mice by flow cytometry and senescence markers (*p16^{Ink4a}* and *p21^{Cip1}* mRNA) and SASP (*Tnf*, *Mcp1* (also known as *Ccl2*), *Il6* and *Il1b* mRNA)^{14,28,29} were quantified. As expected, expression of *Ercc1* was significantly reduced in these cell types (Extended Data Fig. 3e). *p16* and *p21* were significantly increased in *Vav-iCre^{+/+};Ercc1^{-/-}* mice B cells (B220⁺CD19⁺), T cells (CD3⁺), natural killer cells (CD3⁺NK1.1⁺) and macrophages (CD11b⁺F4/80⁺) compared to littermates (Fig. 1k). SASP expression was increased in T cells, natural killer cells and macrophages in a cell-type specific pattern. Splenocytes, bone marrow cells and peripheral CD3⁺ cells from aged but not young *Vav-iCre^{+/+};Ercc1^{-/-}* mice expressed increased levels of senescence and SASP markers compared to controls, analogous to aged wild-type mice (Fig. 1l, Extended Data Fig. 3f, g). The mRNA expression of *p16* and *p21* was higher in single-cell suspensions from spleens and bone marrow of male mutant mice than female mice^{28,29} (Extended Data Fig. 3h, i). This demonstrates that increased endogenous DNA damage via *Ercc1* deletion causes increased senescence in immune cells.

A downstream consequence of endogenous genotoxic stress is increased levels of reactive oxygen species, leading to further macromolecular damage³. Splenocytes from 5-month-old *Vav-iCre^{+/+};Ercc1^{-/-}* mice had increased levels of superoxide anion (Extended Data Fig. 1c). NRF2 is activated by oxidative stress, but can be lost after chronic stress^{14,30}. The expression of NRF2 (encoded by *Nfe2l2*) and its targets *Cat*, *Nqo1* and *Hmox1* were significantly increased in 5-month-old mutant mice compared to controls, but not in younger mice (Extended Data Fig. 1d, e). In older *Vav-iCre^{+/+};Ercc1^{-/-}* mice, *Nfe2l2* expression was significantly lower than controls, comparable to aged wild-type mice (Extended Data Fig. 1d, e). Catalase activity diminished with age in splenic tissue from *Vav-iCre^{+/+};Ercc1^{-/-}* and wild-type mice (Extended Data Fig. 1f, g). The antioxidant glutathione (GSH) was also reduced in the spleens of *Vav-iCre^{+/+};Ercc1^{-/-}* mice (Extended Data Fig. 1h). Concomitantly, adducts of 4-hydroxynonenal (HNE), a lipid peroxidation product, increased in the spleens of *Vav-iCre^{+/+};Ercc1^{-/-}* mice (Extended Data Fig. 1i). These data reveal increased oxidative stress in lymphoid tissues of *Vav-iCre^{+/+};Ercc1^{-/-}* mice, consistent with accelerated ageing.

To characterize which immune cell subsets were senescent, mass cytometry was performed on splenocytes from 10–12-month-old *Vav-iCre^{+/+};Ercc1^{-/-}* and aged wild-type mice (Fig. 2, Extended Data Fig. 4). viSNE analysis was performed on CD45⁺ cells to determine the expression of p16 and p21 in immune cell populations. viSNE distinguished CD3⁺, CD4⁺ and cytotoxic CD8⁺ T cells, T regulatory (T_{reg}) cells

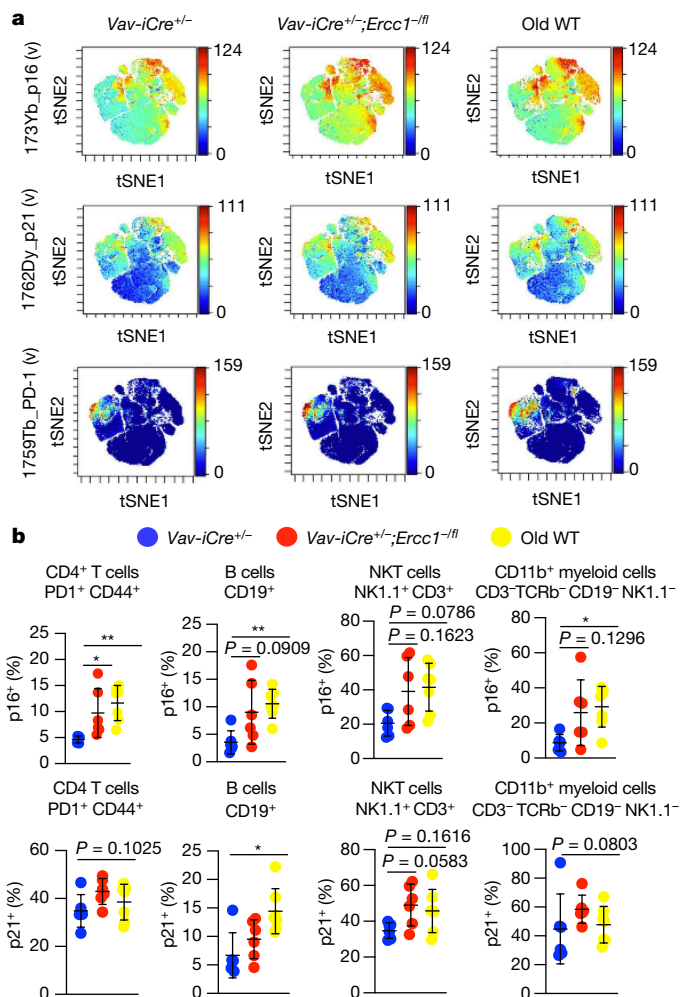


Fig. 2 | Identification of senescent immune cell types by CyTOF.

a, Representative viSNE plots identifying immune cells that express p16 (top), p21 (middle) and PD-1 (bottom) from 10–12-month-old *Vav-iCre^{+/+}* or *Vav-iCre^{+/+};Ercc1^{-/-}* mice, or a 2-year-old wild-type mouse. **b**, Quantification of p16- and p21-expressing immune cell subsets ($n = 6$ *Vav-iCre^{+/+}*; $n = 6$ *Vav-iCre^{+/+};Ercc1^{-/-}*; $n = 7$ 2-year-old WT mice analysed in a single CyTOF experiment). NKT cells, natural killer T cells. Data are mean \pm s.d. * $P < 0.05$, ** $P < 0.01$, Kruskal–Wallis test with Dunn’s correction. See Extended Data Fig. 4 for additional data.

(FOXP3), natural killer cells (NK1.1), B cells (CD19) and CD11b⁺ myeloid cells (Extended Data Fig. 4). The CD11b⁺ myeloid cell cluster appeared particularly enriched for both p16 and p21 in *Vav-iCre^{+/+};Ercc1^{-/-}* mice and aged wild-type mice (Fig. 2a, Extended Data Fig. 4a). Twelve distinct immune cell types were analysed for the expression of p16, p21 and CENP-B senescence markers (Extended Data Fig. 4). The frequency of p16⁺, p21⁺ and CENP-B⁺ cells varied within and between immune cell subsets. Although there was a trend for increased p16⁺, p21⁺ and CENP-B⁺ cells in immune cells from *Vav-iCre^{+/+};Ercc1^{-/-}* mice, significant differences were only detected in T cell subsets for p16 expression (Fig. 2b). CD4⁺CD44⁺PD1⁺ cells exhibited increased expression of p16 and p21, consistent with these being senescence-associated T cells³¹. The frequency of p16⁺, p21⁺ and CENP-B⁺ cells was significantly increased in most immune cell types from two-year-old wild-type mice compared with 10–12-month-old *Vav-iCre^{+/+}* controls (Fig. 2b, Extended Data Fig. 4), whereas in 10–12-month-old *Vav-iCre^{+/+};Ercc1^{-/-}* mice, the frequency of only p16⁺ T cells was significantly increased compared to age-matched *Vav-iCre^{+/+}* controls. Expression of PD-1 was increased in CD4⁺ cells in aged wild-type mice (Fig. 2b). FOXP3⁺, FOXP3⁻ and RORγT⁺

CD4⁺CD44⁺PD-1⁺ subsets had increased p16⁺ cells in *Vav-iCre^{+/+};Ercc1^{-/-}* mice and aged wild-type mice (Extended Data Fig. 4), which indicates increased senescence in T_{reg} cells and non-T_{reg} CD4⁺ cells. B cells, natural killer T cells and CD11b⁺ myeloid cells had increased p16 expression in *Vav-iCre^{+/+};Ercc1^{-/-}* mice compared to age-matched controls (Fig. 1b), consistent with the RNA data (Fig. 1). Aged wild-type mice had significantly increased frequencies of CENP-B⁺ cells for all the populations analysed (Extended Data Fig. 4). This demonstrates that *Vav-iCre^{+/+};Ercc1^{-/-}* and aged wild-type mice have similar, but not identical, subsets of immune cells undergoing senescence.

Senescence in solid organs

To determine whether immune senescence in *Vav-iCre^{+/+};Ercc1^{-/-}* mice affects non-lymphoid organs, tissues were collected from 8–11-month-old mice and DNA damage, oxidative stress and senescence were measured (Fig. 3, Extended Data Figs. 5, 6). The expression of *p16* and *p21* was increased in many tissues of older, but not younger *Vav-iCre^{+/+};Ercc1^{-/-}* mice compared to controls (Fig. 3a, b, Extended Data Fig. 5a). Thus, immune senescence precedes peripheral senescence. *p16* in situ hybridization revealed that p16 expression occurred in non-immune parenchymal cells (Fig. 3c, Extended Data Fig. 5b–e). In the liver, *p16* staining co-localized with the actin-stain phalloidin and albumin-expressing cells with enlarged nuclei, consistent with hepatocytes. In the kidney, the *p16* signal overlapped with cells staining for kidney-specific cadherin, which was expressed in distal tubules and collecting ducts. In the lung, *p16* staining occurred in airway epithelia. Finally, senescence-associated β -galactosidase (SA- β -gal) staining was increased in renal tubules and polyhedral cells in the liver, suggestive of hepatocytes^{6,32} (Extended Data Fig. 5f). The expression of senescence markers was greater in male *Vav-iCre^{+/+};Ercc1^{-/-}* mice than in female mice, consistent with wild-type mice (Extended Data Fig. 5g, h). The liver and, to a lesser extent, kidneys of *Vav-iCre^{+/+};Ercc1^{-/-}* mice had increased oxidative DNA lesions, HNE adducts and oxidized GSH levels (Fig. 3d, Extended Data Fig. 6a–c). These data suggest an aged immune system drives systemic changes associated with normal ageing.

Tissue damage

Notably, the senescence and oxidative stress observed in immune organs of *Vav-iCre^{+/+};Ercc1^{-/-}* mice were sufficient to cause tissue damage in non-deleted organs. Hepatic damage markers alanine and aspartate aminotransferase were increased in serum from *Vav-iCre^{+/+};Ercc1^{-/-}* mice compared to age-matched *Vav-iCre^{+/+}* controls (Fig. 3e). Albumin and kidney damage markers were increased in the urine from *Vav-iCre^{+/+};Ercc1^{-/-}* mice (Fig. 3f, Extended Data Fig. 6d–f). Levels of the pancreatic dysfunction marker amylase were increased in *Vav-iCre^{+/+};Ercc1^{-/-}* mouse serum (Fig. 3g). The above changes also occurred in aged wild-type mice (Fig. 3d–g). The level of glycosaminoglycans, in particular aggrecan, was reduced in the intervertebral discs *Vav-iCre^{+/+};Ercc1^{-/-}* mice (Fig. 3h, Extended Data Fig. 6g, h), characteristic of age-related disc degeneration^{23,33,34}. *p16* expression was significantly increased in immune-privileged tissues such as the intervertebral disc (Extended Data Fig. 6i) and brain (Fig. 3a, b). Histological and molecular evidence of disc ageing was also present (Extended Data Fig. 6j). Regeneration after muscle injury was impaired in *Vav-iCre^{+/+};Ercc1^{-/-}* mice compared to controls (Fig. 3i, Extended Data Fig. 6k) and the ratio of infiltrating M2 to M1 macrophages was significantly reduced (Extended Data Fig. 6l). Grip strength was diminished in older *Vav-iCre^{+/+};Ercc1^{-/-}* mice (Extended Data Fig. 6m). Levels of serum β_2 -microglobulin (Fig. 3j), GDF-15, IL-1 β , MCP-1, osteopontin and TNF were increased in *Vav-iCre^{+/+};Ercc1^{-/-}* and aged wild-type mice (Fig. 3k). Increases in these SASP factors was age-dependent and progressive in the mutant mice (Extended Data Fig. 7a). However, quantification of age-related histopathological lesions in *Vav-iCre^{+/+};Ercc1^{-/-}* mice did not reveal a

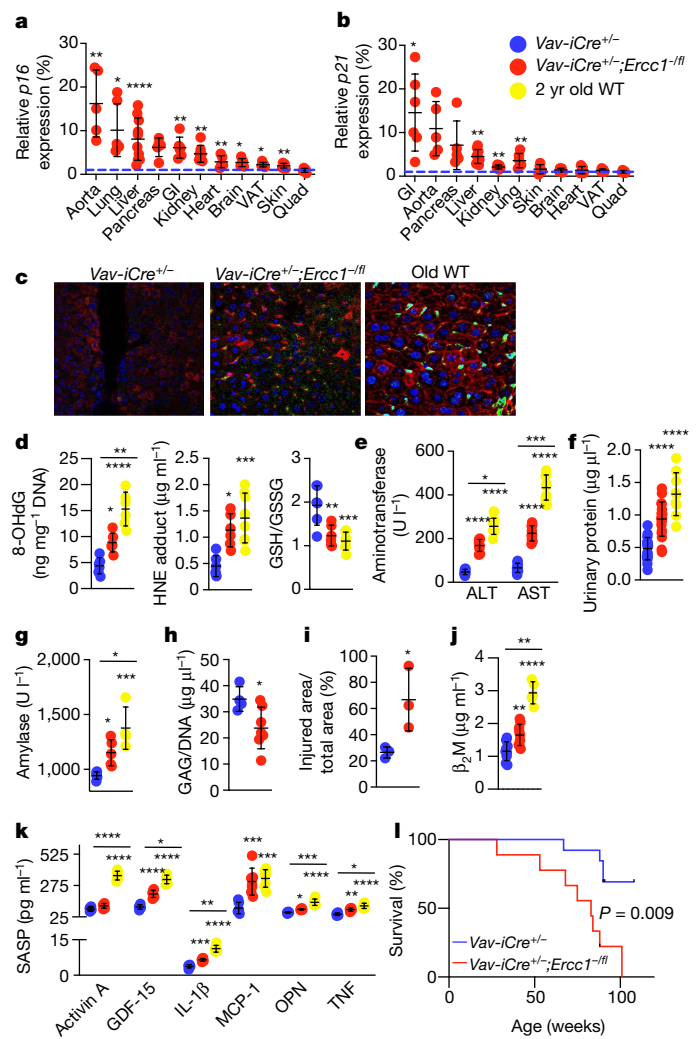


Fig. 3 | An aged immune system drives senescence and loss of tissue homeostasis in non-lymphoid organs. Several senescence and tissue damage markers were measured in 8–11-month-old *Vav-iCre* mice and old wild-type mice (see Supplementary Table 3 for sample size details). **a, b**, Expression of *p16* (**a**) and *p21* (**b**) ($n = 5–10$ mice) in mutant mice was normalized to *Vav-iCre^{+/+}* controls (blue line). GI, gastrointestinal; VAT, visceral adipose tissue. **c**, Representative images of in situ hybridization on hepatic sections for *p16* mRNA (green), albumin (red) to detect hepatocytes, and DAPI (blue nuclei). See also Extended Data Fig. 5. **d**, Hepatic 8-oxo-guanine DNA adducts and HNE protein adducts measured by ELISA ($n = 6–8$ mice per group). Glutathione ratio (reduced glutathione (GSH) to oxidized glutathione (GSSG) ratio) in livers of *Vav-iCre^{+/+};Ercc1^{-/-}* mice ($n = 6$), *Vav-iCre^{+/+}* controls ($n = 6$) and aged wild-type mice ($n = 7$). **e**, Serum aminotransferase levels ($n = 9$ mice per group). ALT, alanine aminotransferase; AST, aspartate transaminase. **f**, Urinary protein levels from *Vav-iCre* ($n = 18$) and old wild-type ($n = 9$) mice measured by Bradford assay. **g**, Serum amylase levels in *Vav-iCre^{+/+};Ercc1^{-/-}* ($n = 5$), *Vav-iCre^{+/+}* ($n = 6$), and old wild-type ($n = 4$) mice. **h**, Glycosaminoglycan (GAG) levels in intervertebral discs of *Vav-iCre^{+/+};Ercc1^{-/-}* ($n = 7$) and *Vav-iCre^{+/+}* ($n = 4$) mice. **i**, Wound area after cardiotoxin injury of the gastrocnemius ($n = 3$ mice per group). **j**, Serum β_2 -microglobulin (β_2M) levels determined by ELISA of *Vav-iCre^{+/+};Ercc1^{-/-}* and *Vav-iCre^{+/+}* mice ($n = 9$ mice per group) and aged wild-type mice ($n = 5$). **k**, Serum SASP protein levels in *Vav-iCre^{+/+};Ercc1^{-/-}* ($n = 6–7$, depending on the protein), *Vav-iCre^{+/+}* controls ($n = 5–6$) and old wild-type ($n = 5–7$) mice, measured by ELISA. **l**, Lifespan of *Vav-iCre^{+/+};Ercc1^{-/-}* ($n = 9$) and *Vav-iCre^{+/+}* ($n = 13$) mice. Data are mean \pm s.d. * $P < 0.05$, ** $P < 0.01$, *** $P < 0.001$, **** $P < 0.0001$, two-tailed unpaired Student's *t*-test (**a, b, h, i**), one-way ANOVA with Tukey's test (**d–g, j, k**), or log-rank (Mantel–Cox) test (**l**).

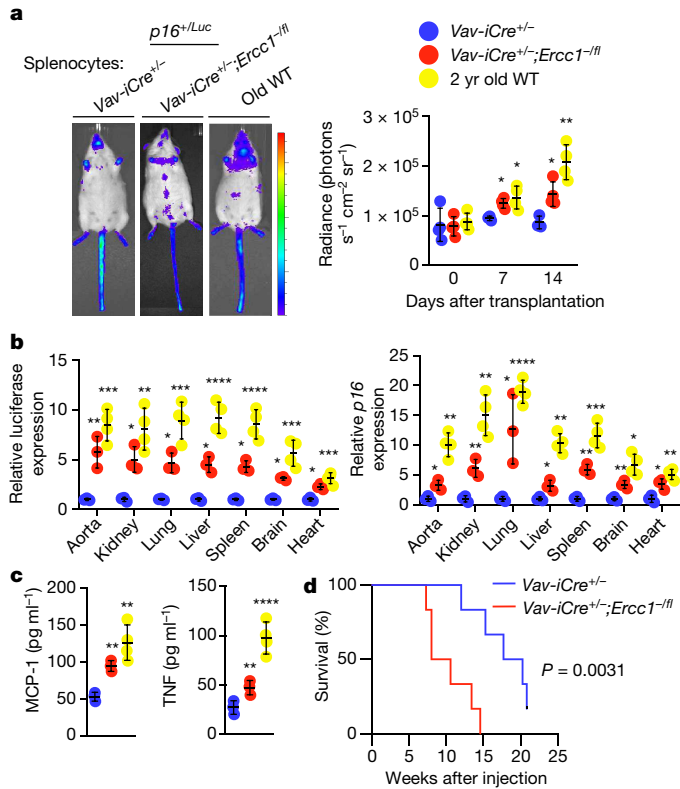


Fig. 4 | Adoptive transfer of splenocytes from $Vav-iCre^{+/-};Ercc1^{fl/fl}$ and aged wild-type mice are sufficient to drive senescence *in trans*. Splenocytes from 8–10-month-old $Vav-iCre^{+/-};Ercc1^{fl/fl}$ mice, $Vav-iCre^{+/-}$ controls, or two-year-old wild-type mice were injected retro-orbitally into 3–4-month-old $p16^{Mk4a/Luc}$ senescence reporter mice ($n = 2$ donor mice per genotype). **a**, Representative images and weekly measures of luminescence in recipient mice ($n = 3$ recipient mice for $Vav-iCre^{+/-};Ercc1^{fl/fl}$ or $Vav-iCre^{+/-}$ splenocytes; $n = 4$ recipients for old WT splenocytes). **b**, Tissues were collected from recipient mice 2 weeks after the final imaging and the expression of the $p16$ - and the $p16$ -driven luciferase reporter were measured by quantitative PCR with reverse transcription (qRT-PCR). **c**, Levels of serum SASP factors MCP-1 (left) and TNF (right) in recipient mice 2 weeks after adoptive transfer. **d**, Lifespan of $Ercc1^{fl/fl}$ mice after adoptive transfer of splenocytes from 19-month-old $Vav-iCre^{+/-};Ercc1^{fl/fl}$ or $Vav-iCre^{+/-}$ ($n = 2$ donors per group) mice. Recipient mice were 2 months of age when transplanted ($n = 5$ for mutant; $n = 6$ for control splenocytes). Data are mean \pm s.d. * $P < 0.05$, *** $P < 0.01$, **** $P < 0.001$, **** $P < 0.0001$, one-way ANOVA with Tukey's test (**b**, **c**), or log rank (Mantel–Cox) test (**d**).

significant increase compared with age-matched $Vav-iCre^{+/-}$ controls (Extended Data Fig. 7b). Finally, the lifespan of $Vav-iCre^{+/-};Ercc1^{fl/fl}$ mice was significantly reduced (Fig. 3). These data demonstrate that an aged immune system can drive the loss of tissue homeostasis, frank damage and age-associated changes in several peripheral organs that contribute to reduced lifespan.

Cell non-autonomous mechanism

To prove that immune cells from $Vav-iCre^{+/-};Ercc1^{fl/fl}$ mice drive secondary senescence and ageing pathology *in trans*, splenocytes were isolated from mutant mice and two-year-old wild-type mice then transplanted into $p16^{Mk4a}$ -luciferase reporter mice³⁵. $Vav-iCre^{+/-};Ercc1^{fl/fl}$ splenocytes had significantly increased levels of luciferase signal at 1 and 2 weeks after transplantation compared to splenocytes from $Vav-iCre^{+/-}$ donors (Fig. 4a). Splenocytes from aged wild-type mice resulted in an even greater induction of luciferase signal. Recipient mice had higher levels of $p16$, $p21$ and luciferase reporter mRNA in

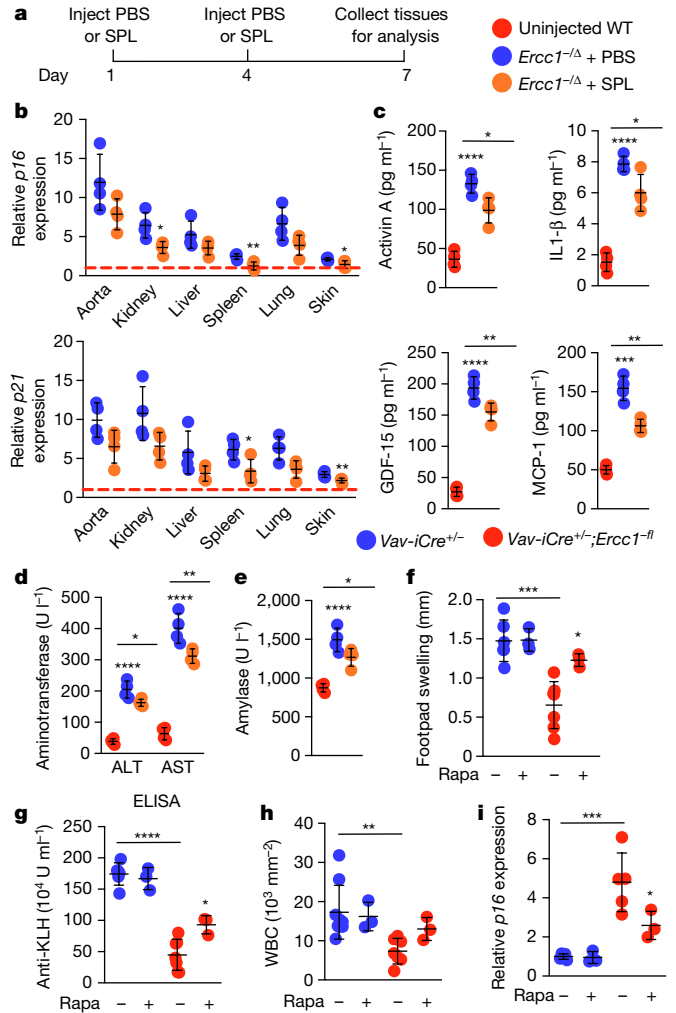


Fig. 5 | Transplantation of splenocytes from young mice suppresses senescence and tissue damage in aged recipients, whereas rapamycin improves immune function of $Vav-iCre^{+/-};Ercc1^{fl/fl}$ mice. **a**, Adoptive transfer: 3-month-old $Ercc1^{fl/fl}$ mice were injected retro-orbitally with 5×10^6 splenocytes (SPL) from 2-month-old wild-type mice ($n = 2$ donors) or vehicle only (PBS) at days 1 and 4. At day 7, tissues were collected from recipient mice ($n = 4$ mice per group) and uninjected age-matched wild-type mice. **b**, Expression of senescence markers $p16$ and $p21$ measured by qRT-PCR. Gene expression was normalized to that of untreated, age-matched wild-type mice (horizontal dashed line). **c**, SASP proteins activin A, GDF-15, MCP-1 and IL-1 β were measured in the serum of recipient mice by single- or multiplex-ELISA. **d**, Serum aminotransferase levels. **e**, Serum amylase levels. **f**, Mice were treated with or without rapamycin (Rapa; 4 mg kg^{-1} intraperitoneally, three times per week) for 6 weeks starting at 3 months of age, followed by 1 week of no drug, then a DTH assay was initiated with KLH (Methods). Footpad swelling was measured 48 h after antigenic challenge ($n = 3/7$ $Vav-iCre^{+/-};Ercc1^{fl/fl}$ or $n = 3/6$ $Vav-iCre^{+/-}$ mice +/- rapamycin, respectively). **g**, One month after DTH challenge, anti-KLH antibodies were measured by ELISA (n values as in **f**). **h**, Peripheral WBC count 1 month after DTH challenge ($n = 3/7$ $Vav-iCre^{+/-}$ and for $Vav-iCre^{+/-};Ercc1^{fl/fl}$ +/- rapamycin, respectively). **i**, Expression of $p16$ in peripheral blood mononuclear cells (PBMCs), measured by qRT-PCR. Data are mean \pm s.d. * $P < 0.05$, ** $P < 0.01$, *** $P < 0.001$, **** $P < 0.0001$, one-way ANOVA (**b**–**e**) or two-way ANOVA (**f**–**i**) with Tukey's test.

several non-lymphoid organs (Fig. 4b, Extended Data Fig. 8a) when administered aged splenocytes (mutant or old wild-type) compared to those from young mice. There were also increased SASP proteins in the serum of recipient mice transplanted with aged splenocytes (Fig. 4c). The increased bioluminescence in recipient reporter mice

persisted for one month (Extended Data Fig. 8b). Transplanted splenocytes were found in several organs of recipient mice regardless of the donors (Extended Data Fig. 8c). Transplantation of splenocytes from *Vav-iCre^{+/+};Ercc1^{-/-}* mice into progeroid *Ercc1^{-/-}* mice significantly reduced their lifespan (Fig. 4d), reinforcing the conclusion that the aged or senescent immune cells drive accelerated ageing and the decreased lifespan of *Vav-iCre^{+/+};Ercc1^{-/-}* mice (Fig. 3l).

Cell autonomous mechanism

The data above suggest that aged splenocytes can drive cell non-autonomous senescence in several tissues through a gain-of-function mechanism. To determine whether a loss-of-function mechanism also contributes, splenocytes from young wild-type mice were transplanted into *Ercc1^{-/-}* mice and the expression of senescence markers was measured one month after transplantation (Extended Data Fig. 9a). Splenocytes from young mice reduced senescence in several tissues of *Ercc1^{-/-}* mice (Extended Data Fig. 9b) and levels of circulating SASP factors (Extended Data Fig. 9c). More acutely, two doses of young splenocytes (Fig. 5a) reduced *p16* and *p21* mRNA in tissues from *Ercc1^{-/-}* recipient mice (Fig. 5b), circulating SASP factors (Fig. 5c) and markers of tissue damage (alanine aminotransferase, aspartate aminotransferase or amylase) (Fig. 5d, e). These data support a loss-of-function mechanism in which aged immune cells are unable to suppress senescence.

Rapamycin rejuvenates immune cells

Inhibition of mTOR activity with a rapamycin analogue in elderly people enhances their response to influenza vaccination and reduces infection rates^{11,12}, which indicates that immunosenescence can be modulated. To determine whether *Vav-iCre^{+/+};Ercc1^{-/-}* mice model this, mice were treated with rapamycin and immune function was measured. Footpad swelling, titres of anti-KLH serum and white blood cell counts were increased in rapamycin-treated *Vav-iCre^{+/+};Ercc1^{-/-}* mice compared to untreated controls (Fig. 5f–h, Extended Data Fig. 9d). Expression of *p16* and *p21* in CD3⁺ peripheral T cells was reduced by rapamycin, as were serum levels of MCP-1 and TNF (Fig. 5i, Extended Data Fig. 9e, f), which suggests modulation of both the gain- and loss-of-function mechanisms by which immune senescence drives systemic ageing.

The key conclusions from this study are that immune cells are vulnerable to endogenous DNA damage, which if unrepaired causes cell death or senescence. Senescence in the immune compartment, as occurs with normal ageing, affects innate and adaptive immunity, in particular follicular helper T cell and natural killer cell function, and potentially drives senescence and age-related changes in solid organs. The mechanism behind parenchymal damage appears to be a combination of cell autonomous (loss-of-function) and cell non-autonomous (gain-of-function, for example, SASP). We conclude that targeting senescent immune cells with senolytic drugs has great potential for suppressing multi-morbidities of old age.

Online content

Any methods, additional references, Nature Research reporting summaries, source data, extended data, supplementary information, acknowledgements, peer review information; details of author contributions and competing interests; and statements of data and code availability are available at <https://doi.org/10.1038/s41586-021-03547-7>.

- Kennedy, B. K. et al. Geroscience: linking aging to chronic disease. *Cell* **159**, 709–713 (2014).
- St Sauver, J. L. et al. Risk of developing multimorbidity across all ages in a historical cohort study: differences by sex and ethnicity. *BMJ Open* **5**, e006413 (2015).
- Robinson, A. R. et al. Spontaneous DNA damage to the nuclear genome promotes senescence, redox imbalance and aging. *Redox Biol.* **17**, 259–273 (2018).
- Wang, J., Clauson, C. L., Robbins, P. D., Niedernhofer, L. J. & Wang, Y. The oxidative DNA lesions 8,5'-cyclopurines accumulate with aging in a tissue-specific manner. *Aging Cell* **11**, 714–716 (2012).
- Baker, D. J. et al. Naturally occurring p16^{INK4a}-positive cells shorten healthy lifespan. *Nature* **530**, 184–189 (2016).
- Zhu, Y. et al. The Achilles' heel of senescent cells: from transcriptome to senolytic drugs. *Aging Cell* **14**, 644–658 (2015).
- Xu, M. et al. Senolytics improve physical function and increase lifespan in old age. *Nat. Med.* **24**, 1246–1256 (2018).
- Pettan-Brewer, C. & Treuting, P. M. Practical pathology of aging mice. *Pathobiol. Aging Age Relat. Dis.* **1**, (2011).
- Bumgardner, S. A. et al. Genetic influence on splenic natural killer cell frequencies and maturation among aged mice. *Exp. Gerontol.* **104**, 9–16 (2018).
- Liu, Y. et al. Expression of p16^{INK4a} in peripheral blood T-cells is a biomarker of human aging. *Aging Cell* **8**, 439–448 (2009).
- Mannick, J. B. et al. mTOR inhibition improves immune function in the elderly. *Sci. Transl. Med.* **6**, 268ra179 (2014).
- Mannick, J. B. et al. TORC1 inhibition enhances immune function and reduces infections in the elderly. *Sci. Transl. Med.* **10**, eaaq1564 (2018).
- Olshansky, S. J. Articulating the case for the longevity dividend. *Cold Spring Harb. Perspect. Med.* **6**, a025940 (2016).
- van Deursen, J. M. The role of senescent cells in ageing. *Nature* **509**, 439–446 (2014).
- Kirkland, J. L. & Tchankonia, T. Cellular senescence: a translational perspective. *EBioMedicine* **21**, 21–28 (2017).
- Goronzy, J. J. & Weyand, C. M. Understanding immunosenescence to improve responses to vaccines. *Nat. Immunol.* **14**, 428–436 (2013).
- Krishnamurthy, J. et al. *Ink4a/Arf* expression is a biomarker of aging. *J. Clin. Invest.* **114**, 1299–1307 (2004).
- Vicente, R., Matusset-Bonnefont, A. L., Jorgensen, C., Louis-Plence, P. & Brondello, J. M. Cellular senescence impact on immune cell fate and function. *Aging Cell* **15**, 400–406 (2016).
- Pinti, M. et al. Aging of the immune system: Focus on inflammation and vaccination. *Eur. J. Immunol.* **46**, 2286–2301 (2016).
- Cho, J. S., Kook, S. H., Robinson, A. R., Niedernhofer, L. J. & Lee, B. C. Cell autonomous and nonautonomous mechanisms drive hematopoietic stem/progenitor cell loss in the absence of DNA repair. *Stem Cells* **31**, 511–525 (2013).
- Gregg, S. Q. et al. A mouse model of accelerated liver aging caused by a defect in DNA repair. *Hepatology* **55**, 609–621 (2012).
- Lavasani, M. et al. Muscle-derived stem/progenitor cell dysfunction limits healthspan and lifespan in a murine progeria model. *Nat. Commun.* **3**, 608 (2012).
- Nasto, L. A. et al. Genotoxic stress accelerates age-associated degenerative changes in intervertebral discs. *Mech. Ageing Dev.* **134**, 35–42 (2013).
- Niedernhofer, L. J. et al. A new progeroid syndrome reveals that genotoxic stress suppresses the somatotroph axis. *Nature* **444**, 1038–1043 (2006).
- Siegemund, S., Shepherd, J., Xiao, C. & Sauer, K. *hCD2-iCre* and *Vav-iCre* mediated gene recombination patterns in murine hematopoietic cells. *PLoS ONE* **10**, e0124661 (2015).
- Su, Y., Orelli, B., Madireddy, A., Niedernhofer, L. J. & Schärer, O. D. Multiple DNA binding domains mediate the function of the ERCC1-XPF protein in nucleotide excision repair. *J. Biol. Chem.* **287**, 21846–21855 (2012).
- Sharpe, A. H. & Pauken, K. E. The diverse functions of the PD1 inhibitory pathway. *Nat. Rev. Immunol.* **18**, 153–167 (2017).
- Sharpless, N. E. & Sherr, C. J. Forging a signature of in vivo senescence. *Nat. Rev. Cancer* **15**, 397–408 (2015).
- Coppé, J. P., Desprez, P. Y., Krtolica, A. & Campisi, J. The senescence-associated secretory phenotype: the dark side of tumor suppression. *Annu. Rev. Pathol.* **5**, 99–118 (2010).
- Zhang, H., Davies, K. J. A. & Forman, H. J. Oxidative stress response and Nrf2 signaling in aging. *Free Radic. Biol. Med.* **88** (Pt B), 314–336 (2015).
- Shimatani, K., Nakashima, Y., Hattori, M., Hamazaki, Y. & Minato, N. PD-1^{hi} memory phenotype CD4⁺ T cells expressing C/EBP β underlie T cell immunodepression in senescence and leukemia. *Proc. Natl Acad. Sci. USA* **106**, 15807–15812 (2009).
- Zhao, J. et al. Quantitative analysis of cellular senescence in culture and in vivo. *Curr. Protoc. Cytom.* **79**, 9.51.1–9.51.25 (2017).
- Munshi, R. et al. MCP-1 gene activation marks acute kidney injury. *J. Am. Soc. Nephrol.* **22**, 165–175 (2011).
- Argyropoulos, C. P. et al. Rediscovering β -2 microglobulin as a biomarker across the spectrum of kidney diseases. *Front. Med. (Lausanne)* **4**, 73 (2017).
- Burd, C. E. et al. Monitoring tumorigenesis and senescence in vivo with a p16^{INK4a}-luciferase model. *Cell* **152**, 340–351 (2013).

Publisher's note Springer Nature remains neutral with regard to jurisdictional claims in published maps and institutional affiliations.

© The Author(s), under exclusive licence to Springer Nature Limited 2021

Methods

Data reporting

No statistical methods were used to predetermine sample size. The mice were randomly assigned to experimental groups, except in experiments that required specific genotypes and ages, and investigators were blinded to allocation during experiments and outcome assessment, except for rare instances in which blinding was not possible.

Animals

Vav-iCre mice (obtained from The Jackson Laboratory, strain name B6.Cg-Tg(*Vav1-icre*)^{A2Kio/J}) were previously described²⁵. The cDNA for exons 8–10 of *Ercc1* along with a neomycin cassette all flanked by *loxP* sites was inserted into the *Ercc1* locus in frame with exon 7 to create a floxed allele of *Ercc1* (Supplementary Fig. 2a). *Ercc1*^{+/β} FVB/N mice were crossed with C57BL/6J *Vav-iCre*^{-/-}; *Ercc1*^{+/-} mice to create *Vav-iCre*^{+/-}; *Ercc1*^β mice carrying one knockout and one floxed allele excised by codon improved Cre (iCre) recombinase in haematopoietic cells (Supplementary Fig. 2b). Wild-type mice were purchased from Jackson Laboratory. *Ercc1*^{-Δ} mice were bred as previously described³⁶. *p16*-luciferase reporter mice were obtained from Ohio State University³⁵. All experimental mice maintained were in an F₁ background from two inbred parents (FVB/N and C57BL/6J) to create congenic mice without strain-specific pathology. Ear punches were used for animal identification and genotyping by TransnetYX. Mice were group housed in ventilated micro-isolator cages on Allentown racks. Mouse cages were changed every two weeks. Mice were handled in a HEPA filtered laminar flow hood with gloves and forceps that were disinfected between cages, and bedding and equipment were autoclaved. All mice were fed irradiated chow (Teklad Global Soy Protein-Free Rodent diet 2020), and chlorinated water was provided through the Edstrom Reverse Osmosis (RO) automatic watering system supplied to the racks through water manifolds. All animal studies were conducted in compliance with the US Department of Health and Human Services Guide for the Care and Use of Laboratory Animals and were approved by The Scripps Research Institute and University of Minnesota Institutional Animal Care and Use Committee.

RNA isolation and qRT-PCR

Gene expression analysis was performed as previously described^{3,37}. Tissues were collected from euthanized mice and flash-frozen in liquid nitrogen. Tissues were homogenized using FastPrep-24 homogenizer (MP Biomedicals) and total RNA was isolated by Trizol extraction according to manufacturer's specifications (Thermo Fisher). Total RNA was quantified using a Nanodrop spectrophotometer (Thermo Fisher) and 1 μg of total RNA used to generate cDNA via the Transcriptor First Strand cDNA synthesis kit (Roche) according to the manufacturer's specifications. Gene expression changes in *p16*^{Ink4a}, *p21*^{Cip1}, *Il6*, *Mcp1* and *Tnf* were quantified by qRT-PCR reactions using 20 μl reaction volumes and a StepOne thermocycler (Thermo Fisher) with input of 50 ng total RNA per reaction (except *p16*^{Ink4a}, 100 ng total RNA). For each sample, reactions were performed in duplicate. Data were analysed by the ΔΔC_t method and expression was normalized to *Gapdh*. Primer sequences are as follows: *B2m* Fwd 5'-CGGCTGTATGCTATCCAGA-3', *B2m* Rev 5'-GGGTGAATTCAGTGTGAGCC-3'; *Cdkn1a* (*p21*^{Cip1}) Fwd 5'-GTCA GGCTGGTCTGCCTCCG-3', *Cdkn1a* (*p21*^{Cip1}) Rev 5'-CGGTCCCGTGGACAGT GAGCAG-3'; *Cdkn2a* (*p16*^{Ink4a}) Fwd 5'-CCCAACGCCCGAACT-3', *Cdkn2a* (*p16*^{Ink4a}) Rev 5'-GCAGAAGAGCTGCTACGTGAA-3'; *Ercc1* Fwd 5'-AAAAGCTGGAGCAGA-3', *Ercc1* Rev 5'-AAGAGCTGTTCCAGGG AT-3' *Gapdh* Fwd 5'-AAGGTCATCCAGAGCTGAA-3', *Gapdh* Rev 5'-CTG CTCACCACCTTCTTGA-3'; *Il6* Fwd 5'-CTGGAAATCGTGAAT-3', *Il6* Rev 5'-CCAGTTTGGTAGCATCCATC-3'; *Mcp1* Fwd 5'-GCATCCACGT GTTGCTCA-3', *Mcp1* Rev 5'-CTCCAGCCTACTCATTGGGATCA-3'; *Tnf* Fwd 5'-ATGAGAAGTCCCAAATGGC-3', *Tnf* Rev 5'-CTCCAC TTGGTGGTTTGCTA-3'; *Hmox1* Fwd 5'-AGAATGCTGAGTTCATGAAGAA-3',

Hmox1 Rev 5'-CTGCTTGTGCGCTCTATCTC-3'; *Nqo1* Fwd 5'-TG CTATGAACTTCAACCCCA-3', *Nqo1* Rev 5'-GCGTCCTCCTTATATGCT-3'; *Nfe2l2* Fwd 5'-GCTTTTGGCAGAGACATTCC-3', *Cat* Fwd 5'-ATA GCCAGAAGAGAAACCCCA-3', *Cat* Rev 5'-TTCATGTGCCGGTGACCAT-3'; Firefly luciferase Fwd 5'-GCCATGAAGCGCTACGCCCTGG-3', luciferase Rev 5'-TCTTGCTACGAATACGACGGTGG-3'.

Isolation of peripheral blood CD3⁺ T cells

Isolation of CD3⁺ T cells was performed as previously described³⁷. Blood was obtained from mice by cardiac puncture, immediately placed into 1/10th volume of 0.5 M EDTA and gently mixed to prevent coagulation. Samples were centrifuged at 300g for 10 min in a tabletop centrifuge. Supernatant was discarded and the cell pellet was suspended in 1 ml ACK buffer (150 mM NH₄Cl, 10 mM KHCO₃, 0.1 mM Na₂EDTA, pH 7.4) to lyse red blood cells and then incubated at room temperature for 10 min. Cells were spun down and ACK lysis was repeated for a second time. Cells were then spun down, washed in 1× Dulbecco's PBS (DPBS), and resuspended in 1× DPBS with 0.5% FBS and 2 mM EDTA. Then, 50 μl of CD3-biotin conjugate (Miltenyi Biotech) was added to the cell suspension solution and incubated for 30 min on ice. Cells were centrifuged at 100g for 10 min and washed twice in resuspension buffer. The cell pellet was then resuspended in 500 μl of resuspension buffer and 100 μl of anti-biotin microbeads added before a 15-min incubation on ice. Cells were washed twice, resuspended in 500 μl of resuspension buffer and applied to MACS column attached to a magnet. Cells were washed with three column volumes of buffer before elution. Cells were centrifuged and RNA isolation was conducted using a RNeasy kit (Qiagen) according to manufacturer's specifications. qRT-PCR analysis of senescence markers was performed as indicated above.

Immunoblotting

Snap-frozen livers from mice were incubated in RIPA buffer (Thermo-Fisher) on ice for 30 min after being homogenized with a FastPrep-24 homogenizer. Samples were centrifuged at 17,000g for 15 min at 4 °C. Supernatant was resuspended in 2× SDS loading buffer and 50 μg of total protein run on a 4–15% SDS-PAGE gel (Bio-Rad) before being transferred to nitrocellulose membrane. Membranes were blocked for 1 h in 10% milk TBS-T solution at room temperature before incubation in anti-ERCC1 (Santa Cruz Biotechnology, sc-17089), anti-γH2AX (Novus Biologicals, NB100-384, 1:2,000) and anti-GAPDH (Abcam, ab8425, 1:5,000) antibody at 4 °C overnight. After washing, samples were incubated in either horse anti-mouse HRP (Cell Signaling Technology, 7076S) or goat anti-rabbit HRP secondary antibody (Thermo-Fisher, 656120, 1:2,000) in 5% milk TBS-T solution for 3 h before washing and visualization with ECL (Thermo-Fisher).

Fluorescent in situ hybridization

Detection of *p16* mRNA was performed as previously described^{6,37,38}. In brief, liver, lung and kidney sections were deparaffinized, rehydrated and boiled in sodium citrate buffer. Slides were prehybridized in a 4× SSC solution containing 3% BSA at 55 °C. Slides were then incubated with either a scrambled non-specific probe or a custom-designed *p16* LNA probe (5'-TCTCATGCCATTTCCTTCTCTGT-3', Exiqon) diluted in hybridization buffer containing 10% dextran sulfate in 4× SSC. Slides were hybridized at 55 °C for 1 h and then submitted to a series of five washes of decreasing stringency. Sections were imaged using confocal scanning laser microscopy.

SA-β-gal staining

Fresh tissues from 8–11-month-old *Vav-iCre*^{+/-}; *Ercc1*^β and littermate controls were fixed in 10% neutral buffered formalin (NBF) for 3–4 h and then transferred to 30% sucrose overnight. Tissues were then embedded in cryo-embedding medium (OCT) and cryosectioned at 5 μm for staining of SA-β-gal (pH 6.0) at 37 °C for 16–24 h in SA-β-gal staining solution (40 mM citric acid in sodium phosphate buffer, 5 mM K₄[Fe(CN)₆]

Article

3H₂O, 5 mM K₃[Fe(CN)₆], 150 mM sodium chloride, 2 mM magnesium chloride and 1 mg ml⁻¹ X-gal dissolved in *N,N*-dimethylformamide). Slides were imaged at 20× with a Panoptiq slide scanner (ViewSiq).

Multiplex analysis of SASP factors

Quantitation of SASP factor abundance was performed as previously described^{37,39}. Serum levels of SASP were measured in *Vav-iCre^{+/+};Ercc1^{-fl}* and littermate controls (*n* = 3–9 mice per group) at different ages using a multiplex assay using the Milliplex Map Mouse Metabolic Hormone Magnetic Bead Panel kit (MCP-1 and TNF) (Millipore Sigma). Serum (10 µl) of serum was analysed in duplicate and analyte concentrations were quantified on a Luminex 200 (Luminex Corporation) microplate reader. Serum levels of IL-1β, activin A, GDF-15 and osteopontin were measured by single-analyte ELISA (Abcam; R&D Systems) using a Varioskan plate reader (Thermo-Fisher).

Body weight and NMR measurement of body composition

A Bruker LF minispec body composition analyser (Bruker) was used to measure body composition of mice (11–25 mice per group). Body weights were measured by use of a standard top loader balance (Ohaus) and body composition was investigated by using non-invasive nuclear magnetic resonance technique to rapidly measure the percentage fat, lean mass and fluid in non-anaesthetized mice.

Comprehensive blood counts

Tail bleeds from mice were analysed using a SciL Vet ABC Plus (Henry Schein Animal Health) or HemaTrue (Heska) haematology analyser.

Analysis of functional markers

Serum levels of amylase (pancreatic dysfunction), alanine aminotransferase and aspartate aminotransferase (liver damage markers) were quantified by ELISA (Abcam) using a Varioskan plate reader (Thermo-Fisher).

Adoptive transfers and in vivo imaging detection of luciferase activity

Approximately 5 × 10⁶ splenocytes were obtained from 8–10-month-old *Vav-iCre^{+/+}* and *Vav-iCre^{+/+};Ercc1^{-fl}* and 2-year-old wild-type mice. Red blood cells were lysed in ACK buffer and then cells were washed in 1 × DPBS and resuspended in 100 µl of 1 × DPBS before being retro-orbitally injected into 3–4-month-old isoflurane-anaesthetized *p16^{Ink4+/Luc}* mice. Isoflurane-anaesthetized mice were subcutaneously injected with 10 µl per gram body weight D-luciferin substrate (Caliper Life Sciences; 15 mg ml⁻¹ in 1 × DPBS) and were imaged weekly using an IVIS Lumina (PerkinElmer) as previously described^{35,37}.

Immune cell transplantations into progeroid mice

Approximately 5 × 10⁶ splenocytes were obtained from 2-month-old wild-type mice. Red blood cells were lysed in ACK buffer and then cells were washed in 1 × DPBS and resuspended in 100 µl of DBPS before being retro-orbitally injected into 3-month-old isoflurane-anaesthetized *Ercc1^{-d}* mice. Mice were euthanized one month later, and tissues collected for the senescence marker analysis and circulating SASP factors.

Homologous immune cells in recipient mice

Splenocytes (10 × 10⁶ cells) from 7- or 26-month old wild-type male mice were retro-orbitally injected into 7-month-old female recipient mice. Twenty-four hours after injection, tissues were collected and snap-frozen in liquid nitrogen. DNA was isolated using DNeasy blood and tissue kit (Qiagen) as specified by the manufacturer. Equivalent amounts of total DNA for each sample in a specific tissue was used to amplify the Sry gene by PCR. PCR products were electrophoresed in a gel containing SYBR Safe (Thermo-Fisher) and imaged on an iBright gel imager (Thermo-Fisher).

Sry Fwd 5'-TTGTCTAGAGAGCATGGAGGGCCATGTCAA-3', *Sry* Rev 5'-CCACTCCTCTGTGACACTTTAGCCCTCCGA-3'.

Histopathology

Tissues were collected from euthanized mice and fixed in 10% neutral buffered formalin. Tissues were processed and paraffin embedding before sectioning (4-µm thickness). Sections were stained with haematoxylin and eosin. Specimens were interpreted by a board-certified veterinary pathologist for age-related pathology.

Geropathology

The Geropathology Grading Platform (GGP) is a grading system to assess mouse biological ageing through the measurement of pathological status of several tissues using a standardized scoring system. The scoring system generates a numerical score for the total lesions in each tissue, which are then averaged in each mouse to generate a composite lesion score (CLS)⁴⁰.

Delayed-type hypersensitivity measurements

Mice were sensitized by a 100 µl subcutaneous injection of freshly prepared KLH antigen (2 mg ml⁻¹) emulsified 1:1 in Freund's complete adjuvant (Thermo-Fisher). The emulsion was mixed by forcing the adjuvant-immunogen mixture through a small orifice. Two weeks later after sensitization, anaesthetized mice were challenged by injecting 20 µg of KLH dissolved in 10 µl of 1 × DPBS or 1 × DPBS vehicle only in rear footpads. The mice were monitored to ensure they regained consciousness before being returned to their cages. Paw thickness of each hind paw was monitored with a spring-loaded caliper (Dyer) at 0, 24, 48 and 72 h after antigen administration. Only the 0 h point was measured under anaesthesia.

Anti-KLH antibodies ELISA

Serum obtained from mice in the DTH experiments was analysed for the presence of mouse anti-KLH antibodies using the anti-KLH IgG ELISA (Life Diagnostics Inc.) and a SpectraMax plate reader (Molecular Devices). Blood samples were collected from the tail vein.

Peripheral blood and lymphoid analysis by flow cytometry

The spleens and bone marrow were converted into single-cell suspensions and washed with sterile PBS. Red blood cells were depleted with red blood cell lysis buffer (150 mM ammonia chloride, 1 mM sodium bicarbonate and 0.1 mM EDTA at pH 7.7) and the cells were extensively washed before being passed through a cell strainer. Subsequently, the cells were re-suspended in FACS buffer (2% FBS, 1 × PBS, 2 mM EDTA and 0.04% sodium azide) at 3.75 × 10⁶ cells per ml. A 200 µl aliquot of each sample was transferred into 96-well polypropylene round-bottom plates (BD Bioscience). To minimize background noise, Fc receptors were blocked using anti-CD16/CD32 monoclonal antibody (1:600 dilution; purchased from BD Pharmingen) for 20 min at 10 °C. The cells were stained with fluorochrome conjugated monoclonal antibody (purchased from either BD Pharmingen or eBioscience) at the appropriate titre for 45 min at 10 °C. The cells were washed with FACS buffer twice and fixed using 2% paraformaldehyde. For intracellular staining, the cells were processed using a cytofix/cytoperm buffer kit purchased from BD Pharmingen and used according to the manufacturer's instructions. Whole blood was collected in heparinized tubes and analysed as described above after red blood cell lysis. The samples were processed on a BD LSR II flow cytometer (BD Bioscience) and analysed using Flowjo software (Tristar, Inc.). The absolute number of each cell type was calculated by multiplying the percentage calculated by the total splenic cell number.

Sorting of immune cell populations

Bone marrow and splenocytes were obtained from 5-month-old *Vav-iCre^{+/+}* and *Vav-iCre^{+/+};Ercc1^{-fl}* mice. Samples were incubated in ACK

lysis buffer to lyse red blood cells before being washed in 1× DPBS before incubating in Fc block for 15 min on ice. Splenocytes were stained with CD3-PE and NK1.1-FITC for 30 min on ice to sort T and natural killer cells. Bone marrow was stained with CD19-APC, B220-FITC, F4/80-PE-Cy7 and CD11b-PE purchased from either BD Pharmagins or eBioscience) to sort B cells and macrophages. Cells (5×10^4) were sorted into FBS using a BD Aria III flow cytometer. Sorted cells were washed in 1× DPBS and snap frozen in liquid nitrogen. Total RNA was isolated from cells using RNeasy kit and analysed for the expression of senescence and SASP markers as described above.

Natural killer cell cytotoxicity assay

Spleens collected from 8–12-month-old mice were pressed through a 70- μ m filter using a 3 ml syringe filter and rinsed through in 1× DPBS. Samples were centrifuged at 1,000 rpm for 10 min in a tabletop centrifuge. Supernatant was discarded and the cell pellet was suspended in 1 ml ACK buffer (150 mM NH_4Cl , 10 mM KHCO_3 , 0.1 mM Na_2EDTA , pH 7.4) to lyse red blood cells and then incubated on ice for 5 min. Cells were then spun down, washed in 1× DPBS, and resuspended in 1× DPBS with 0.5% FBS and 2 mM EDTA. Then, 50 μ l of anti-CD3–biotin conjugate (Miltenyi Biotech) was used added to the cell suspension solution and incubated for 30 min on ice. Cells were centrifuged at 1,000 rpm for 10 min and washed twice in resuspension buffer. The cell pellet was then resuspended in 500 μ l of resuspension buffer and 100 μ l of anti-biotin microbeads added before a 15 min incubation on ice. Cells were washed twice and then resuspended in 500 μ l of resuspension buffer and applied to MACS column attached to a magnet. Column elution fraction was collected and then centrifuged and resuspended and incubated with 50 μ l anti-NK1.1–biotin conjugate on ice for 30 min. Cells were washed with three column volumes of buffer before elution. Cells were then counted to determine ‘effector’ natural killer cell numbers for use in cytotoxicity assays. Approximately 1×10^6 K562 ‘target’ cells were incubated in 2 ml of complete medium with 20 μ l of 3 mM DiOC₁₈ stain for 1 h at 37 °C. Cells were then washed twice in 1× DPBS to washout the remaining DiOC₁₈ stain and resuspend in cells in complete medium at a density of 1×10^6 per ml. Suspensions of effector cells were prepared in complete medium to yield effector:target ratios of 15:1, 5:1 and 0:1 by mixing 130 μ l of effector cells with 10 μ l of target cells. The cell volume was increased to 995 μ l and 5 μ l of 10 mg ml⁻¹ DAPI propidium iodide solution was added, followed by incubation at 37 °C for 4 h. Cells were washed in 1× DPBS three times and lysis was measured by flow cytometry.

CytoF analysis

Maxpar reagents including water, cell staining buffer (CSB), cell acquisition solution, Cell-ID Intercalator-Ir, Fix and Perm Buffer and EQ Four Element Calibration Beads were purchased from Fluidigm. The eBiosciences FoxP3/Transcription Factor staining buffer set was used for fixation/permeabilization and purchased from (Thermo Fisher). Antibodies used for cell surface labelling and phenotyping were either purchased directly from Fluidigm or purchased from the designated manufacturer (Supplementary Information). Custom-conjugated antibodies were generated in-house through the Mayo Clinic Hybridoma Core using Maxpar X8 antibody labelling kits (Fluidigm) according to the manufacturer’s protocol.

Isolated splenocytes were resuspended in 1 ml of CSB. Samples were then washed twice with CSB. An antibody cocktail of the extracellular markers was prepared as a master mix before adding 50 μ l of cocktail to samples resuspended in 50 μ l of CSB. Samples were then incubated at room temperature for 45 min. After washing twice with CSB, cells were permeabilized with fixation/permeabilization buffer (eBioscience). Afterwards, samples were washed and resuspended in CSB before the addition of a cocktail of intracellular antibody markers and incubation at room temperature for 45 min. Cells were washed and then fixed with 2% PFA for 30 min. Cells were resuspended in intercalation solution

with Perm/Fix buffer (Fluidigm) and incubated overnight at 4 °C. On the next morning, cells were washed with PBS and resuspended in a 1:10 solution of calibration beads and CAS at a concentration of 0.5×10^6 cells ml⁻¹. Before data acquisition, samples were filtered through a 35- μ m blue cap tube (Falcon).

Samples were loaded onto a Helios CyTOF system (Fluidigm) using an attached autosampler and were acquired at a rate of 200–400 events per second. Data were collected as FCS files using the CyTOF software (version 6.7.1014). After acquisition, intrafile signal drift was normalized to the acquired calibration bead signal using the CyTOF software. CyTOF fcs files were analysed using Flowjo version 10 using the gating strategy shown in Supplementary Fig. 5. Generation of graphs and statistical analysis were performed in GraphPad Prism 8. Statistical significance was determined by performing a non-parametric Kruskal–Wallis test along with Dunn’s correction for multiple comparisons. viSNE analysis was performed using Cytobank software. CD45⁺ cells from all 19 samples were equally sampled for a total of 1,299,999 events and the analysis was performed with 3,000 iterations and a perplexity of 50. We used 15 channels for the analysis: TCR β , CD3e, CD62L, CD4, CD8, CD44, GATA3, FOXP3, Tbet, ROR γ T, CD25, CD19, CD11b, CD11c and NK1.1. viSNE illustrations were generated in Cytobank.

Measurement of cyclopurine lesions

DNA was isolated from tissues, which was pulverized with a mortar and pestle under liquid nitrogen. Cyclopurine lesions were measured by liquid chromatography–triple mass spectrometry (LC–MS/MS/MS) using an LTQ linear ion trap mass spectrometer using our recently described conditions with some modifications. Nuclease P1 (0.1 U μ g⁻¹ DNA), phosphodiesterase 2 (0.000125 U μ g⁻¹ DNA), 20 nmol of *erythro*-9-(2-hydroxy-3-nonyl)adenine EHNA and a 20- μ l solution containing 300 mM sodium acetate (pH 5.6) and 10 mM zinc chloride were added to isolated nuclear DNA. In this context, EHNA served as an inhibitor for deamination of 2’-deoxyadenosine to 2’-deoxyinosine induced by adenine deaminase. The above digestion mixture was incubated at 37 °C for 48 h. Alkaline phosphatase (0.05 U μ g⁻¹ DNA), phosphodiesterase 1 (0.00025 U μ g⁻¹ DNA) and 40 μ l of 0.5 M Tris–HCl buffer (pH 8.9) were then added. The digestion was continued at 37 °C for 2 h and subsequently neutralized by the addition of formic acid. Then, appropriate amounts of uniformly ¹⁵N-labelled standard lesions were added, which included *R*-cdG, *S*-cdG, *R*-cdA and *S*-cdA. The digestion mixture was subsequently extracted twice with chloroform. The resulting aqueous layer was subjected to off-line high-performance liquid chromatography (HPLC) separation for the enrichment of the lesions under study, as previously described.

The LC–MS/MS/MS experiments were conducted using an LTQ linear ion trap mass spectrometer. In brief, a 0.5×150 mm Zorbax SB–C18 column (particle size, 5 μ m, Agilent) was used for the separation of the above-enriched lesion fractions, and the flow rate was 4.0 μ l min⁻¹. A solution of 0.1% (v/v) formic acid in water (solution A) and a solution of 0.1% (v/v) formic acid in methanol (solution B) were used as mobile phases for the analyses of all four cyclopurine lesions—that is, the (*S*′*R*) and (*S*′*S*) diastereomers of cdA and cdG, after HPLC enrichment, and a gradient of 5 min 0–20% B, 30 min 20–80% B, and 5 min 80% B was used for the separation.

EPR quantification of O₂^{•-}

Spleen tissue (25 mg) was homogenized in ice-cold HBSS (pH 7.4) containing 100 mM DTPA. The homogenate was then exposed to the EPR hydroxylamine spin probe CMH (1-hydroxy-3-methoxycarbonyl-2,2,5,5-tetramethylpyrrolidine), 200 mM, for 10 min at 25 °C and then centrifuged at 1,000g and the supernatant (50 ml) was placed into an EMXnano EPR cavity for analysis. Controls were performed with added superoxide dismutase (purified CuZnSOD) to validate signal from O₂^{•-}. Values for signal intensity are arbitrary units of signal intensity taken from the up-field peak of the characteristic three-line spectrum from the nitrogen splitting.

Measurement of splenic catalase activity

Catalase activity was measured as previously described³ by detection of hydrogen peroxide at 240 nm using a Cary 300 BIO UV-VI (Varian) spectrophotometer at 30 s intervals for a total of 1 min. Catalase activity per milligram of protein ($k\text{ mg}^{-1}$) was quantified using the following formula: $k\text{ mg}^{-1} = [3\ln(A_{\text{initial}}/A_{\text{final}})]/[\text{milligrams of protein} \times \text{time}]$.

Quantitation of 8-oxo-guanine DNA lesions

Tissues from mice were analysed for 8-oxo-guanine levels using the ELISA kit (Abcam) according to manufacturer's specifications.

Lipid peroxidation products

Tissues from mice were analysed for HNE adducts using the OxiSelect HNE Adduct Competitive ELISA kit (Cell Biolabs) according to manufacturer's specifications as previously described³.

Quantification of glutathione

Fresh tissues from mice were immediately homogenized in 5% sulfosalicylic acid and subsequently analysed for the concentration of reduced (GSH) and oxidized (GSSG) glutathione using the Glutathione Assay Kit (Cayman Chemical) as previously described³.

Short-course rapamycin administration

Three-month-old *Vav-iCre^{+/+}* and *Vav-iCre^{+/+};Ercc1^{-/-}* mice were given intraperitoneal injections of 4 mg kg⁻¹ rapamycin (LC Laboratories) that was formulated with 5% PEG-400 and 5% Tween-80 every other day for six weeks. Mice were given one week for washout before beginning delayed-type hypersensitivity experiments as described above.

β_2 -microglobulin measurement

Analysis of serum and urinary levels of β_2 -microglobulin was performed by ELISA (Abcam) as specified by the manufacturer.

Intervertebral disc aggrecan immunofluorescence

Mouse lumbar intervertebral disc tissue were isolated from spines and fixed overnight at 4 °C in 2% paraformaldehyde. For immunofluorescent staining, the tissues were cryoprotected with 30% sucrose in PBS overnight at 4 °C, then embedded in OCT (Tissue-Tek). Serial axial plane cryosections were cut at thicknesses of 5 μm . The tissue sections were rehydrated in PBS, permeabilized and blocked with 0.25% Triton X-100, 10% goat serum and 1% BSA in PBS for 30 min at room temperature. Incubation with anti-aggrecan (AB1031, Millipore) was carried out overnight at 4 °C following blocking. The sections were then incubated with secondary antibodies (Cy3-conjugate Goat anti-rabbit IgG, Jackson Laboratory) for 60 min at room temperature, according to the manufacturer's protocols. Immunostained sections were imaged and analysed using a Nikon instrument A1 confocal laser microscope and NIS-elements microscopy imaging software.

1,9-Dimethylmethylene blue (DMMB) colorimetric assay for sulfated glycosaminoglycans

For each mouse, nucleus pulposus tissue isolated from four lumbar IVDs of each mouse were pooled and digested using papain at 60 °C for 2 h. GAG content was measured in duplicates by the DMMB procedure using chondroitin-6-sulfate (Millipore Sigma C-8529) as a standard⁴¹. The DNA concentration of each sample was measured using the PicoGreen assay (Molecular Probes) and used to normalize the glycosaminoglycan values.

Muscle injury

Cardiotoxin (CTX; 4 μM , Millipore Sigma, C9759) was injected intramuscularly into the gastrocnemius muscles of the recipient mice. Five days after injury, the mice were euthanized, and the muscles were collected

and flash-frozen in liquid nitrogen-cooled 2-methylbutane. Serial 10- μm cryosections were then stained with haematoxylin and eosin (H&E) for the identification of the injury area. Image acquisition was performed with a Nikon Eclipse Ci at 2-20 \times magnification. To measure the injured area, at least six random 2 \times magnification fields were blindly measured with Image J.

Grip strength analysis

Body weights were collected for each mouse and grip strength was measured using a BIO-GS3 grip strength meter (Bioseb).

Immunohistochemistry

Cryosections from CTX and non-CTX injured muscle were fixed with 5% formalin, blocked with 5% donkey serum, and then incubated with antibodies specific for CD68 (marker of M1 macrophages, ab53444, 1:200, Abcam) and CD163 (marker of M2 macrophages, Sc-33560, 1:50, Santa Cruz) were used to evaluate the ratio of M1/M2 macrophages as a parameter for inflammation in the muscle. Alexafluor 594-conjugated anti-rabbit IgG (1:500; Invitrogen, A21207) and Alexafluor 488-conjugated anti-rat IgG (1:500; Invitrogen, A21208) were used as secondary antibodies. The nuclei were stained with DAPI. All the stained sections were visualized on a Nikon Eclipse Ni-E fluorescence microscope. Ten random pictures per slide were taken and they were blindly measured with Image J.

Schematics

All mouse images in schematics found in figures and extended data figures were adapted from BioRender.

Reporting summary

Further information on research design is available in the Nature Research Reporting Summary linked to this paper.

Data availability

Reasonable requests for all data presented in this Article will be honoured by the corresponding authors.

- Ahmad, A. et al. ERCC1-XPF endonuclease facilitates DNA double-strand break repair. *Mol. Cell. Biol.* **28**, 5082–5092 (2008).
- Yousefzadeh, M. J. et al. Mouse models of accelerated cellular senescence. *Methods Mol. Biol.* **1896**, 203–230 (2019).
- Tabibian, J. H., O'Hara, S. P., Splinter, P. L., Trussoni, C. E. & LaRusso, N. F. Cholangiocyte senescence by way of N-ras activation is a characteristic of primary sclerosing cholangitis. *Hepatology* **59**, 2263–2275 (2014).
- Yousefzadeh, M. J. et al. Circulating levels of monocyte chemoattractant protein-1 as a potential measure of biological age in mice and frailty in humans. *Aging Cell* **17**, e12706 (2018).
- Ladiges, W. Pathology assessment is necessary to validate translational endpoints in preclinical aging studies. *Pathobiol. Aging Age Relat. Dis.* **6**, 31478 (2016).
- Farndale, R. W., Buttle, D. J. & Barrett, A. J. Improved quantitation and discrimination of sulphated glycosaminoglycans by use of dimethylmethylene blue. *Biochim. Biophys. Acta* **883**, 173–177 (1986).

Acknowledgements This work was supported by the National Institutes of Health (NIH) grants P01 AG043376 (P.D.R., L.J.N., E.E.K., J.H.), R01 AG063543 (L.J.N.), R56 AG059676 (L.J.N.), U19 AG056278 (P.D.R., L.J.N., W.C.L.), P01 AG062413 (P.D.R., L.J.N.), R56 AG058543 (W.C.L.), R01 AG044376 (N.V.V.) and the Glenn Foundation (L.J.N., C.E.B.). M.J.Y. is supported by The Irene Diamond Fund/American Federation on Aging Research Postdoctoral Transition Award. Mass cytometry and panel design were performed by S. Farwana and K. D. Pavelko at the Mayo Clinic Immune Monitoring Core. We thank J. Zhao, C. Bukata, K. Melos and M. Calubag for their assistance in measuring senescence. All mouse illustrations were made with BioRender.

Author contributions M.J.Y., R.R.F., P.D.R. and L.J.N. conceived and designed the study. M.J.Y., L.A., S.J.M., T.S. and R.D.O. performed most of the mouse manipulations and in vivo physiological analysis. M.J.Y., R.W.B., J.I.K. and M.P.B. performed ex vivo senescence analysis. C.E.B. provided p16-luciferase reporter mice. E.A.W. assisted with the IVIS analysis of p16-luciferase with L.A. and S.J.M. C.E.T. performed and N.F.L. contributed to p16 in situ hybridization studies. R.R.F. performed immune population analysis. M.J.Y. and K.L. prepared samples for and Y.Z. performed and analysed data from CyTOF with assistance from Z.C.S., A.L.B. and I.M.S. M.J.Y. and T.S. performed immune function tests. M.J.Y. and L.A. performed transplantation experiments. M.J.Y. performed and S.E.L., E.E.K., Y.C. and Y.W. contributed to the analysis of oxidative stress and DNA damage analysis. A.L. and J.H. performed analysis of

cardiotoxin-injected muscle tissues. D.W. and Q.D. performed and N.V.V. contributed to intervertebral disc and spine analysis. J.K., S.P.S.P. and W.C.L. performed histopathological analysis and C.A.M. performed the grip strength analysis. M.J.Y. and R.R.F. wrote the manuscript with input from all co-authors. M.J.Y., R.R.F., P.D.R. and L.J.N. oversaw all experimental design, data analysis and manuscript preparation.

Competing interests L.J.N. and P.D.R. are co-founders of NRTK Biosciences, a start-up biotechnology company developing senolytic drugs.

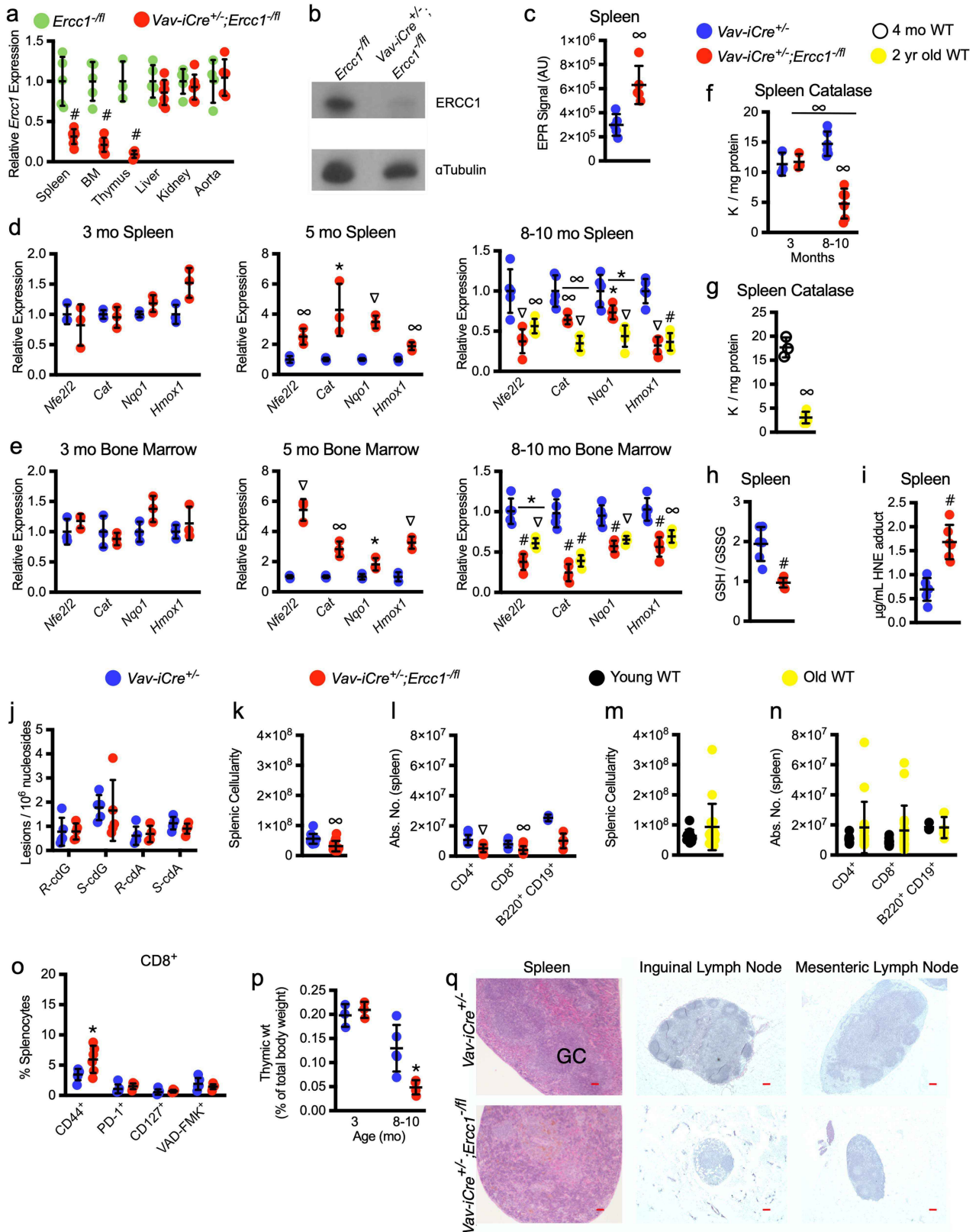
Additional information

Supplementary information The online version contains supplementary material available at <https://doi.org/10.1038/s41586-021-03547-7>.

Correspondence and requests for materials should be addressed to P.D.R. or L.J.N.

Peer review information *Nature* thanks Joan Mannick, Björn Schumacher and the other, anonymous, reviewer(s) for their contribution to the peer review of this work.

Reprints and permissions information is available at <http://www.nature.com/reprints>.

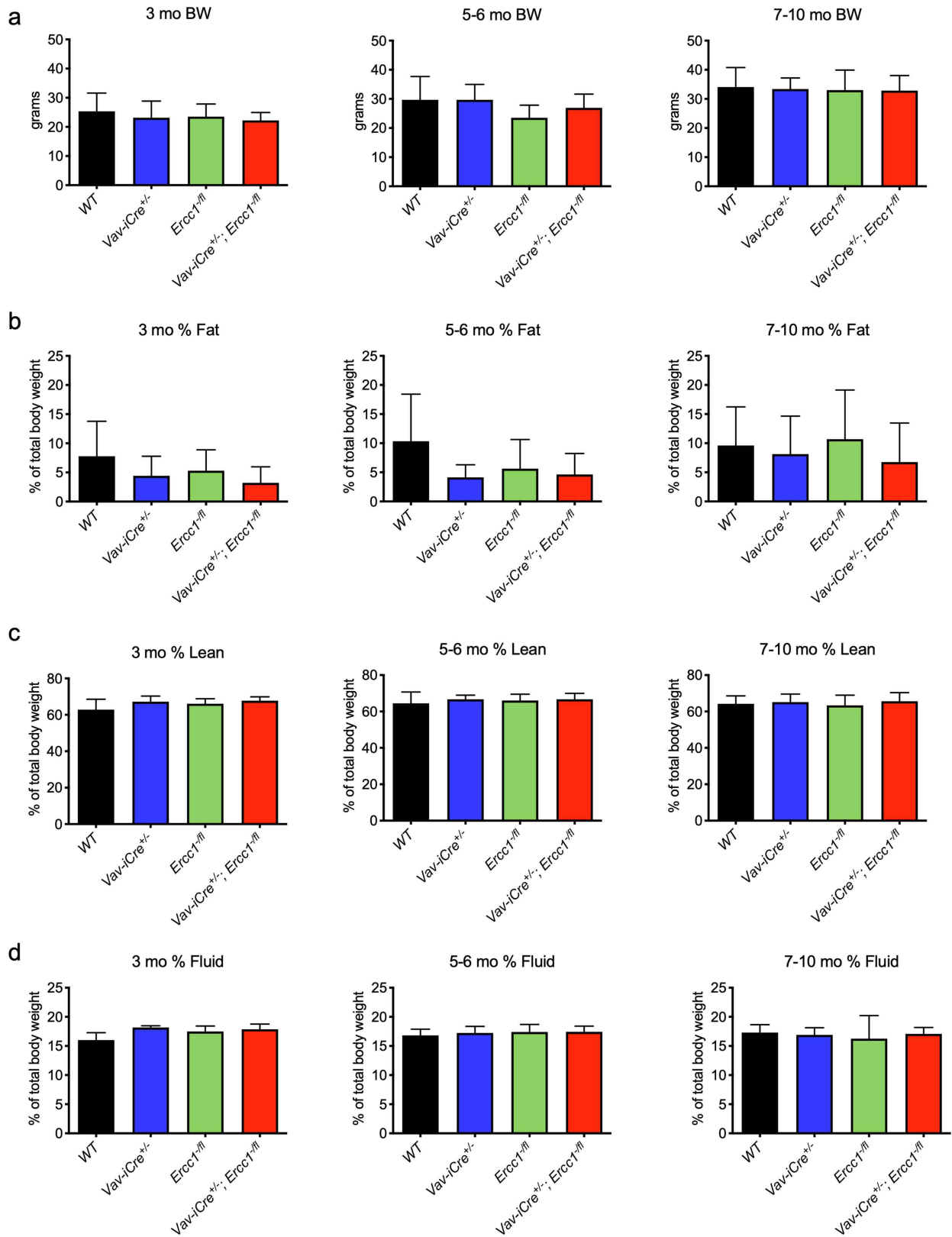


Extended Data Fig. 1 | See next page for caption.

Extended Data Fig. 1 | Molecular changes in *Vav-iCre^{+/+};Ercc1^{fl/fl}* mice.

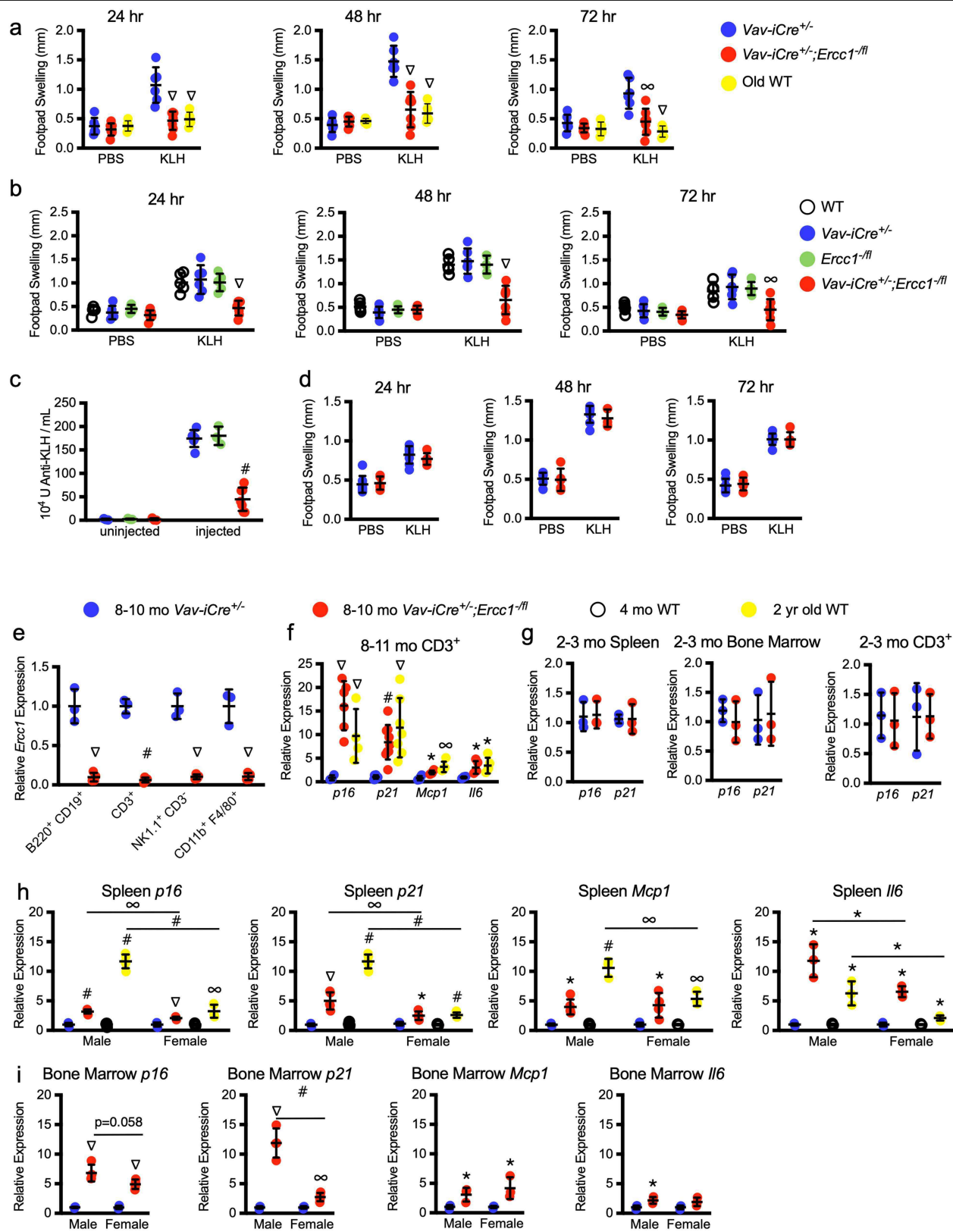
a, Expression of *Ercc1* was measured in tissues from 8–10-month-old *Vav-iCre^{+/+};Ercc1^{fl/fl}* and *Ercc1^{fl/fl}* control mice ($n = 5–7$ *Vav-iCre^{+/+};Ercc1^{fl/fl}*; $n = 3–5$ *Ercc1^{fl/fl}*, depending on the tissue (see Supplementary Table 3 for sample size details). **b**, Detection of ERCC1 in splenic lysates from a 9-month-old *Vav-iCre^{+/+};Ercc1^{fl/fl}* mice and littermate control by immunoblot. **c**, Superoxide anion levels were measured by electron paramagnetic resonance (EPR) in splenic tissue from 6–8-month-old *Vav-iCre^{+/+};Ercc1^{fl/fl}* and littermate control mice ($n = 5$ mice per group). **d, e**, Expression of the transcription factor NRF (*Nfe2l2*) and its downstream targets (*Cat*, *Nqo1*, *Hmox1*) measured by qRT-PCR in spleen (**d**) and bone marrow (**e**) of *Vav-iCre^{+/+};Ercc1^{fl/fl}* and littermate control mice at several ages ($n = 3$ at 3- and 5-months-old; $n = 5$ 8–10-months-old) and in two-year-old wild-type mice ($n = 5$). **f**, Catalase activity measured in splenic tissue from 8–10-month-old *Vav-iCre^{+/+};Ercc1^{fl/fl}* ($n = 6$) and *Vav-iCre^{+/+}* ($n = 3$) mice (Methods). **g**, Catalase activity in 4-month-old ($n = 3$) and 24-month-old ($n = 6$) wild-type mice. **h, i**, The ratio of reduced to oxidized glutathione (GSH/GSSG) (Methods) (**h**) and levels of HNE protein adducts (**i**) measured by ELISA in splenic lysates of *Vav-iCre^{+/+};Ercc1^{fl/fl}* and littermate control mice at 8–11 months of age ($n = 6$ mice per group). **j**, Levels of four cyclopurine adducts in splenic tissue from 8–10-month-old *Vav-iCre^{+/+};Ercc1^{fl/fl}* mice and littermate controls

($n = 4–5$ *Vav-iCre^{+/+};Ercc1^{fl/fl}*; $n = 5$ *Vav-iCre^{+/+}*; see Supplementary Table 3 for sample size details) measured by liquid chromatograph–tandem mass spectrometry (LC–MS/MS/MS) (Methods). **k**, Total splenocyte cell counts from 8–10-month-old *Vav-iCre^{+/+};Ercc1^{fl/fl}* ($n = 14$) mice and *Vav-iCre^{+/+}* ($n = 12$) mice. **l**, The absolute number of T ($CD4^+$, $CD8^+$) and B ($B220^+CD19^+$) cells in spleens from the same mice ($n = 10/4$ *Vav-iCre^{+/+};Ercc1^{fl/fl}*; $n = 8/3$ *Vav-iCre^{+/+}* for $CD4^+$ or $CD8^+$ /B220⁺CD19⁺ measures, respectively) (Methods). **m**, Total splenocyte cell counts from young (7-month-old; $n = 10$) and old (24-month-old; $n = 17$) wild-type mice. **n**, The absolute number of $CD4^+$, $CD8^+$ and B220⁺CD19⁺ cell in spleens from the same mice ($n = 8/3$ young WT; $n = 17/7$ old wild-type mice for $CD4^+$ or $CD8^+$ /B220⁺CD19⁺ measures, respectively). **o**, Analysis of $CD8^+$ splenocytes from 8–10-month-old mice for memory ($CD44^+CD127^+$), exhaustion (PD-1⁺) and apoptosis (VAD-FMK⁺) markers ($n = 6$ mice per group). **p**, Thymic weight normalized to total body weight ($n = 3$ at 3 months old; $n = 4–5$ at 8–10 months old per group). **q**, Histology images (20 \times) of spleen and lymph nodes from 8–10-month-old *Vav-iCre* mice. Scale bar, 100 μ m. GC, germinal centres. Data are mean \pm s.d. * $P < 0.05$, $\infty P < 0.01$, $\nabla P < 0.001$, # $P < 0.0001$, unpaired two-tailed Student's *t*-test (**a, c–e** for the 3- and 5-month-old mice, **g–p**), one-way ANOVA (**d, e** for the 8–10-month-old mice) or two-way (**f**) with Tukey's test.



Extended Data Fig. 2 | *Vav-iCre^{+/-}; Ercc1^{fl/fl}* mice maintain normal weight and body composition. a, Body weight (BW) of three different age groups of mice by genotype. **b–d**, Percentage fat (b), lean mass (c) and fluid (d) measured by

NMR at three ages of mice ($n=8-25$ mice per group) (see Supplementary Table 3 for sample size details). Data are mean \pm s.d. P values (not significant) were determined by one-way ANOVA with Tukey's test.



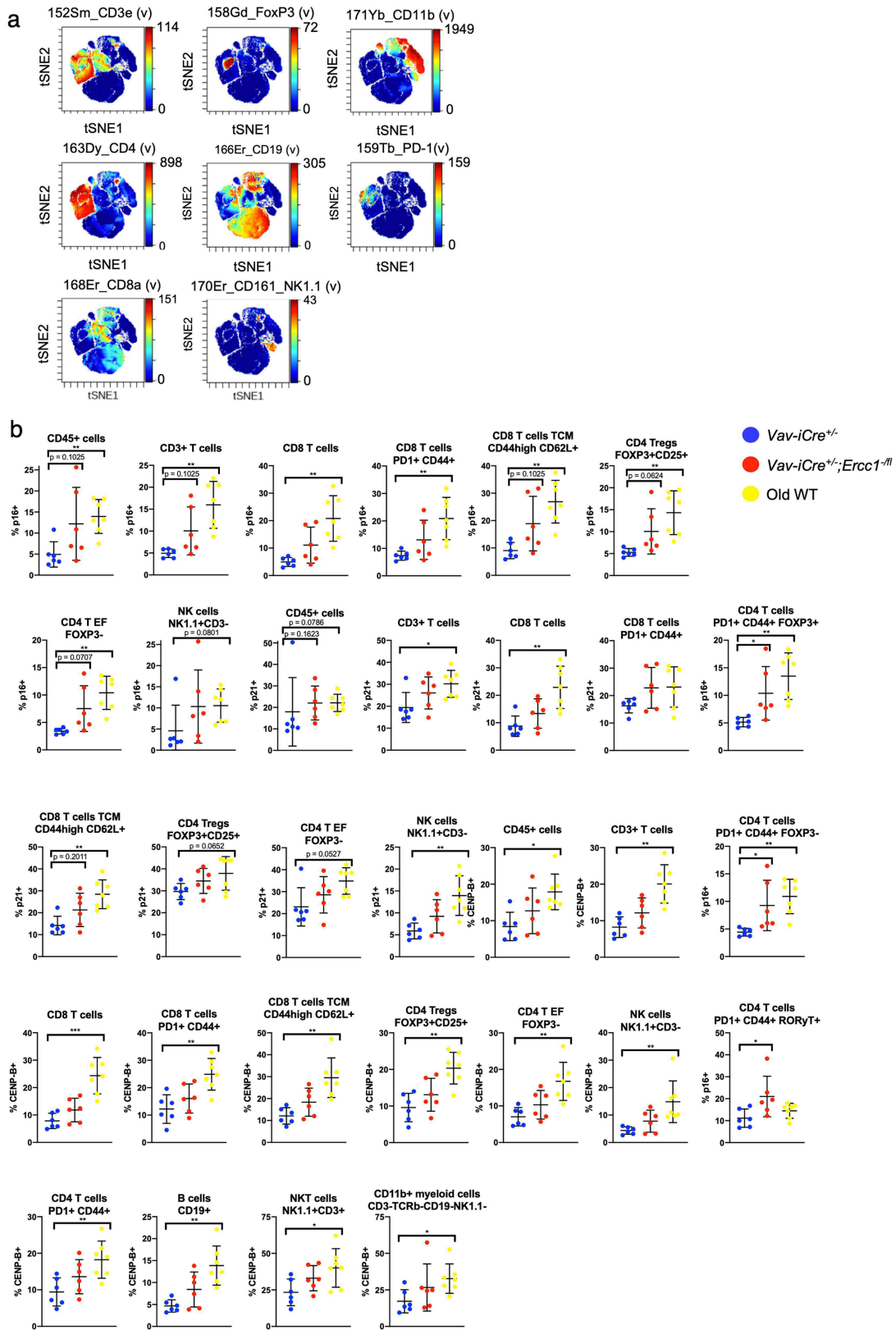
Extended Data Fig. 3 | See next page for caption.

Article

Extended Data Fig. 3 | Measurement of immune function and lymphoid

organ senescence in *Vav-iCre^{+/+};Ercc1^{fl/fl}* mice. **a**, Footpad swelling measurements at several time points after antigenic (KLH) challenge, separated by mouse genotype ($n = 7$ *Vav-iCre^{+/+};Ercc1^{fl/fl}*; $n = 6$ *Vav-iCre^{-/-}*; $n = 5$ old WT mice). **b**, Footpad swelling by genotype ($n = 7$ *Vav-iCre^{+/+};Ercc1^{fl/fl}*; $n = 6$ *Vav-iCre^{+/+}*; $n = 5$ WT mice). **c**, Quantification of anti-KLH antibodies by ELISA one month after antigenic challenge ($n = 3/7$ *Vav-iCre^{+/+};Ercc1^{fl/fl}*; $n = 3/6$ *Vav-iCre^{+/+}*; $n = 3/3$ *Ercc1^{fl/fl}* for naive (uninjected) and KLH-challenged (injected) mice, respectively). **d**, DTH assay in 2-month-old mice *Vav-iCre^{+/+};Ercc1^{fl/fl}* ($n = 5$) and *Vav-iCre^{+/+}* ($n = 8$) controls. Data are mean \pm s.d. $\infty P < 0.01$, $\nabla P < 0.001$, $\#P < 0.0001$, two-way ANOVA with Tukey's test. **e**, Quantification of *Ercc1* expression by qRT-PCR in flow-sorted immune cell populations isolated from spleen (T and natural killer cells) and bone marrow (B cells and macrophages) of 5-month-old *Vav-iCre^{+/+};Ercc1^{fl/fl}* mice and littermate controls ($n = 4$ *Vav-iCre^{+/+};Ercc1^{fl/fl}*; $n = 3$ *Vav-iCre^{+/+}*). Data are mean \pm s.d. $\nabla P < 0.001$, $\#P < 0.0001$,

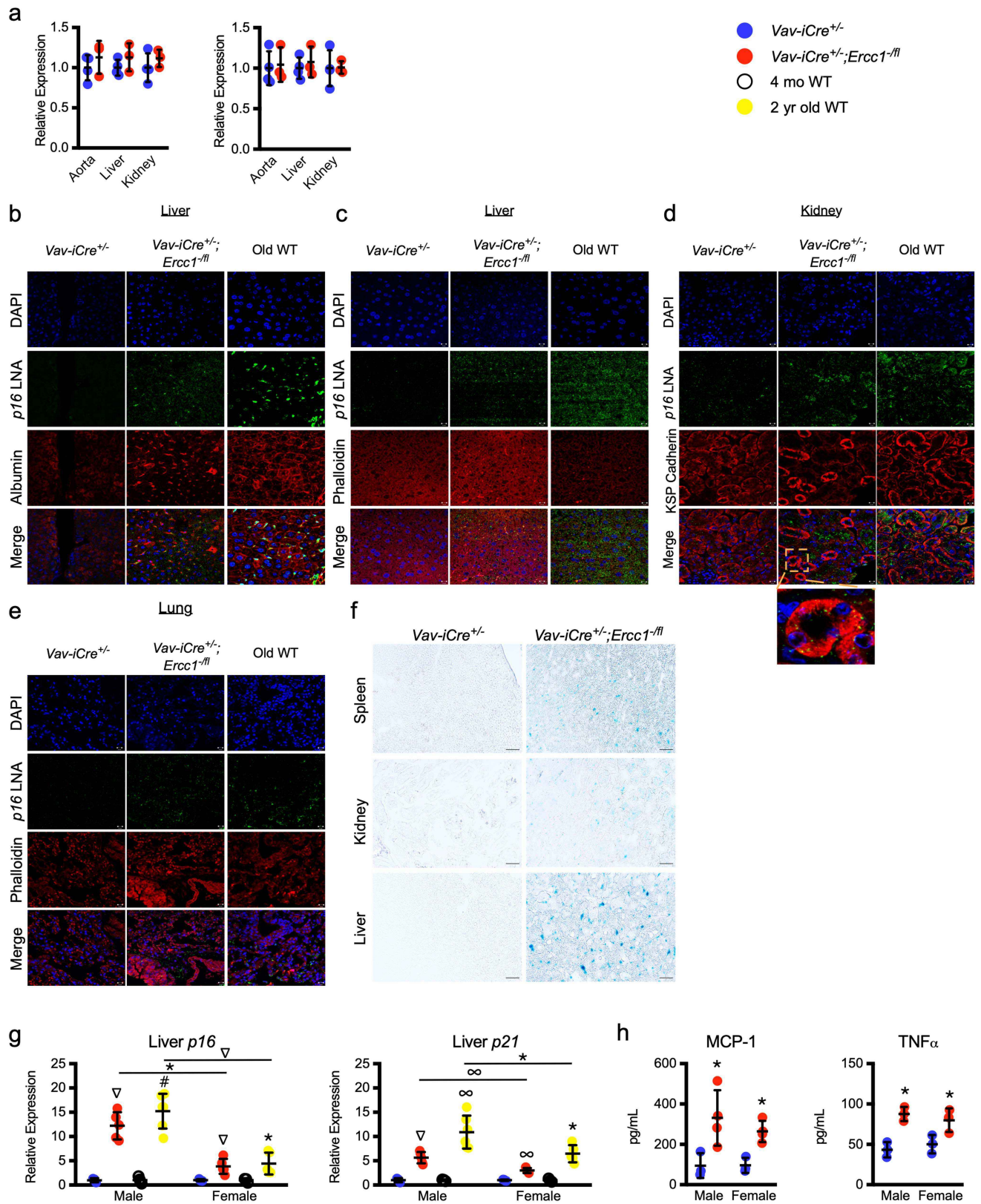
two-tailed unpaired Student's *t*-test. **f**, Senescence marker expression in CD3⁺ peripheral T cells from 8–11-month-old *Vav-iCre* and old wild-type mice ($n = 3–9$ *Vav-iCre^{+/+}*; $n = 6–9$; *Vav-iCre^{+/+};Ercc1^{fl/fl}*; $n = 4–7$ two-year-old wild-type, depending on the gene) (see Supplementary Table 3 for sample size details). **g**, Measurement of senescence marker expression by qRT-PCR in splenic tissue and bone marrow from 2–3-month-old *Vav-iCre* mice ($n = 3$). **h**, Expression of senescence markers in splenic tissue from 8–10-month-old *Vav-iCre^{+/+};Ercc1^{fl/fl}* and old wild-type mice relative to controls by gender ($n = 3–4/3–4$ *Vav-iCre^{+/+}*; $n = 3–5/3–4$ *Vav-iCre^{+/+};Ercc1^{fl/fl}*; $n = 3–6/3–5$ 4-month-old WT; $n = 5/5$ two-year-old WT males/females, respectively) (see Supplementary Table 3 for sample size details). **i**, Expression of senescence markers in bone marrow of *Vav-iCre^{+/+};Ercc1^{fl/fl}* mice ($n = 3–4/3–4$ *Vav-iCre^{+/+}*; $n = 3–4/4–5$ *Vav-iCre^{+/+};Ercc1^{fl/fl}* males/females, respectively). Data are mean \pm s.d. $*P < 0.05$, $\infty P < 0.01$, $\nabla P < 0.001$, $\#P < 0.0001$, unpaired two-tailed Student's *t*-test (**e**, **g**), one-way ANOVA (**f**) or two-way ANOVA (**a–d**, **h**, **i**) with Tukey's test.



Extended Data Fig. 4 | Identification of immune cell types and senescent cells by CyTOF. **a**, viSNE analysis of total CD45⁺ cells to identify immune cell types. Representative viSNE plots are from a *Vav-iCre*^{+/+} control mouse at 10–12 months of age. See Supplemental Fig. 5 for the gating strategy. **b**, The proportion of the indicated immune cell subsets that express p16, p21 or

CENP-B from 10–12-month-old *Vav-iCre*^{+/+};*Ercc1*^{-/-} ($n=6$), *Vav-iCre*^{+/+} ($n=6$), and >2-year-old wild-type ($n=7$) mice was determined by CyTOF. Each dot is an independent mouse. Data are mean \pm s.d. * $P < 0.05$, ** $P < 0.01$, *** $P < 0.001$, Kruskal–Wallis test with Dunn’s correction for multiple comparisons.

Article

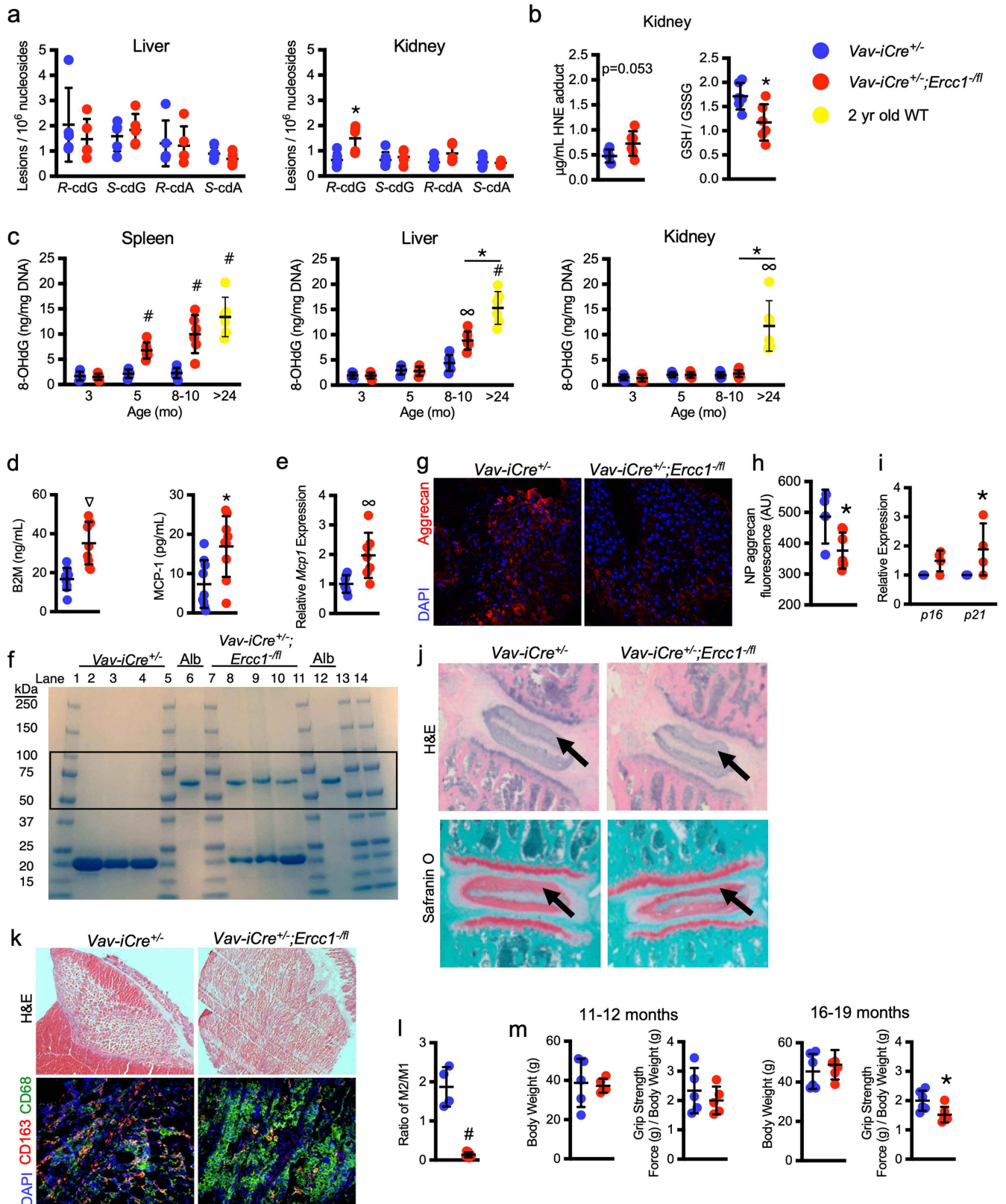


Extended Data Fig. 5 | See next page for caption.

Extended Data Fig. 5 | Co-localization of *p16* mRNA with parenchymal markers in non-lymphoid tissues from *Vav-iCre^{+/+};Ercc1^{fl/fl}* mice.

a, Measurement of senescence marker expression in the organs of 5-month-old *Vav-iCre* mice ($n = 3$ mice per group). **b–e**, Representative images of *p16* in situ hybridization with immunostain or chemical stain for parenchymal markers of liver (**b, c**), kidney (**d**) and lung (**e**) sections from 8–11-month-old *Vav-iCre^{+/+};Ercc1^{fl/fl}* mice, littermate control *Vav-iCre^{+/+}* mice and 2-year-old wild-type mice stained for albumin (liver), phalloidin (liver and lung) or kidney-specific (KSP)-cadherin in the red channel, DAPI (blue), and *p16* LNA probe (green). The full set of images from Fig. 3c is shown in **b**. Original magnification, $\times 40$. Scale bar, $10 \mu\text{m}$. **f**, Representative images of SA- β -gal staining on tissues from 8–10-month-old

Vav-iCre^{+/+};Ercc1^{fl/fl} and littermate controls. Original magnification, $\times 20$. Scale bar, $50 \mu\text{m}$. **g**, Senescence marker expression in the livers of 8–11-month-old *Vav-iCre^{+/+};Ercc1^{fl/fl}* ($n = 5$ male and 4–5 female) (see Supplementary Table 3 for sample size details by gender and gene) and littermate control mice ($n = 3$ male and 3–4 female) as well as 4-month-old ($n = 3$ male and 3–4 female) and 2-year-old ($n = 6$ male and 4–5 female) wild-type mice. **h**, Levels of circulating SASP factor proteins measured by multiplex ELISA in serum from *Vav-iCre^{+/+};Ercc1^{fl/fl}* ($n = 3$ male and 3–4 female) and *Vav-iCre^{+/+}* ($n = 3$ male and 3 female) mice. Data are mean \pm s.d. * $P < 0.05$, $\infty P < 0.01$, $\nabla P < 0.001$, # $P < 0.0001$, unpaired two-tailed Student's *t*-test (**a**) or two-way ANOVA with Tukey's test (**g, h**).

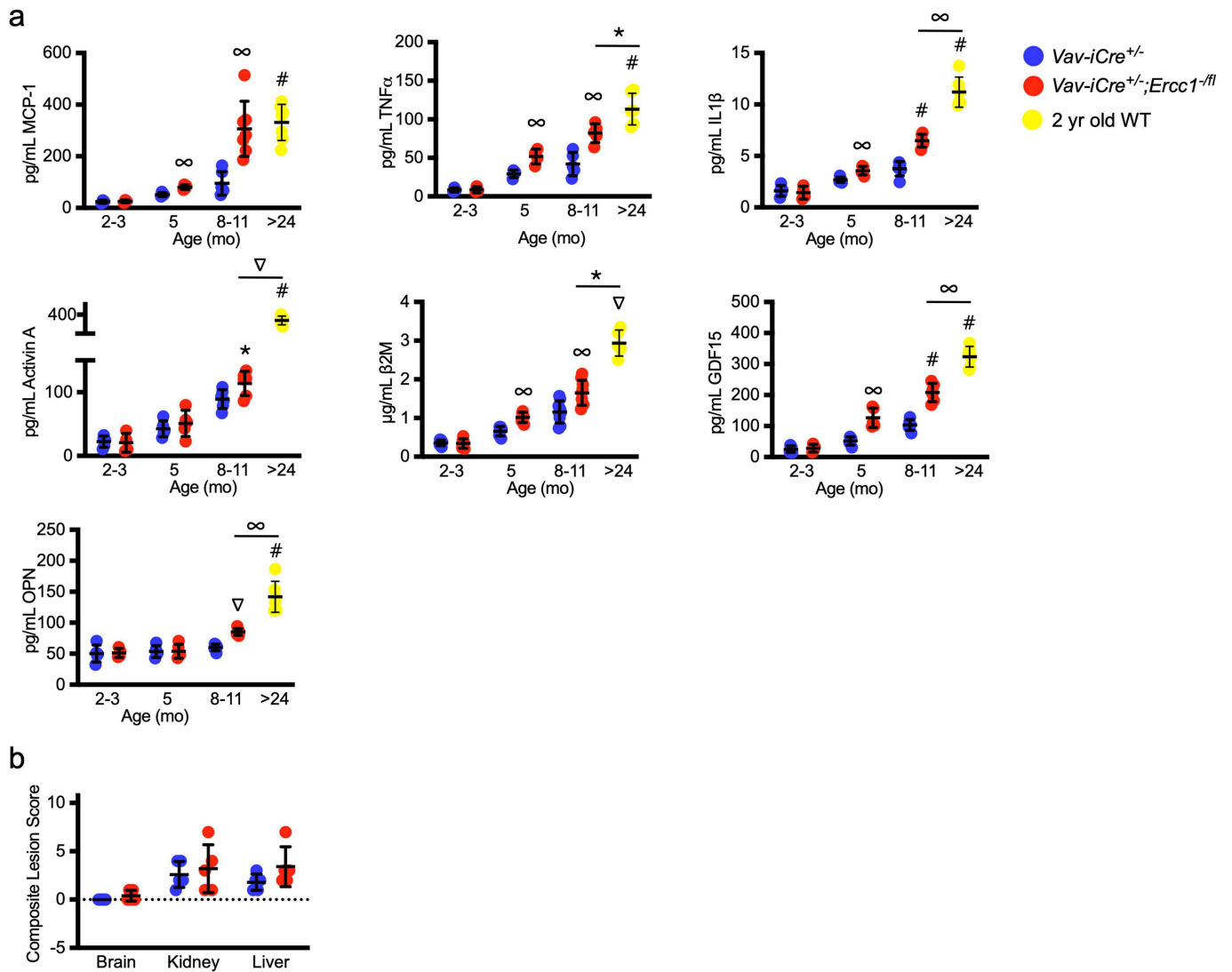


Extended Data Fig. 6 | See next page for caption.

Extended Data Fig. 6 | Cell non-autonomous effects of an aged immune system in non-lymphoid tissues of *Vav-iCre^{+/+};Ercc1^{fl/fl}* mice. **a**, Cyclopurine adducts were measured in the liver and kidneys of 8–11-month-old *Vav-iCre^{+/+};Ercc1^{fl/fl}* ($n = 5$) and littermate control *Vav-iCre^{+/+}* ($n = 5$ for liver and $n = 6$ for kidney) by LC-MS/MS/MS (Methods). **b**, Markers of oxidative stress including HNE protein adducts and the ratio of reduced to oxidized glutathione (GSH/GSSG) measured in the kidneys from 8–11-month-old *Vav-iCre^{+/+};Ercc1^{fl/fl}* and littermate control *Vav-iCre^{+/+}* mice ($n = 6$ mice per group). HNE measure by ELISA. GSH/GSSG measured by chromogenic assay (Methods). **c**, 8-oxo-guanine DNA adducts measured by ELISA in the spleen, liver and kidney of mice at various ages ($n = 5-6/5-6/5$ *Vav-iCre^{+/+};Ercc1^{fl/fl}*; $n = 5-6/5-6/5$ *Vav-iCre^{+/+}*; $n = 5/5/10$ old WT mice for spleen/liver/kidney, respectively) (see Supplementary Table 3 for sample size details by genotype and tissue). **d**, Urinary levels of pro-geronic factor β_2 -microglobulin and MCP-1 measured by ELISA in 8–11-month-old *Vav-iCre^{+/+};Ercc1^{fl/fl}* and littermate controls ($n = 9$ mice per group). **e**, Renal *Mcp1* (also known as *Ccl2*) expression in 8–11-month-old *Vav-iCre^{+/+};Ercc1^{fl/fl}* mice ($n = 7$ per group) measured by qRT-PCR. **f**, Representative Coomassie-stained gel of urine samples from 8–11-month-old *Vav-iCre^{+/+};Ercc1^{fl/fl}* and littermate control mice demonstrating increased proteinuria. Recombinant albumin (Alb) was loaded on the gel as a control

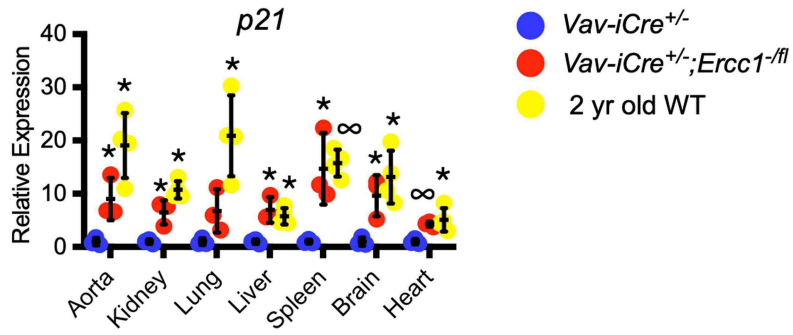
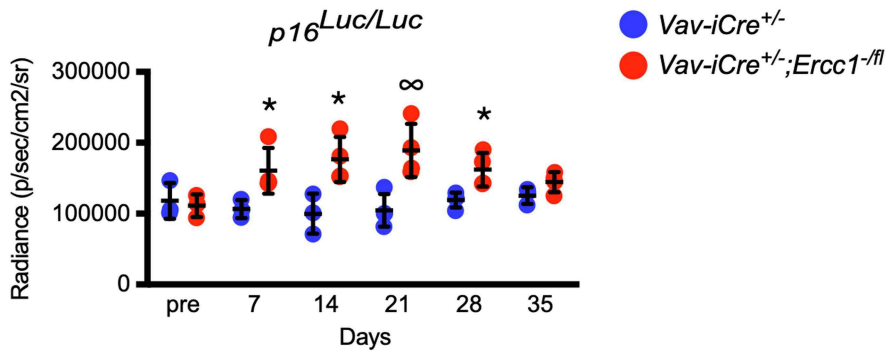
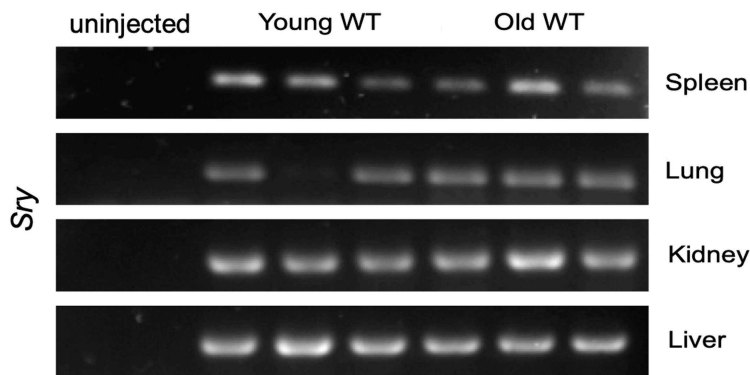
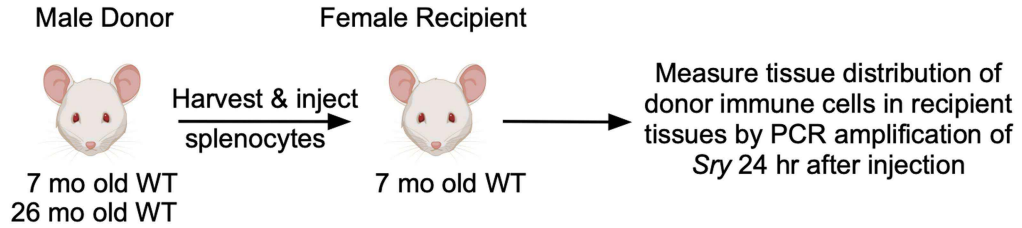
(lanes 6, 12) and its approximate molecular mass denoted by a box (marker ladder lanes 1, 5, 7, 11, 13–14). Each lane represents a unique mouse. **g**, Representative images from tissue sections stained for aggrecan (red) and DAPI (blue) in the nucleus pulposus (NP) of intervertebral discs from 8–11-month-old *Vav-iCre^{+/+};Ercc1^{fl/fl}* and littermate control mice. **h**, Quantification of aggrecan staining ($n = 4$ *Vav-iCre^{+/+}*; $n = 7$ *Vav-iCre^{+/+};Ercc1^{fl/fl}*). **i**, Measurement of senescence marker expression in the intervertebral discs of 8–11-month-old *Vav-iCre^{+/+};Ercc1^{fl/fl}* and littermate control mice ($n = 4$ mice per group) by qRT-PCR. **j**, Representative images of sections of intervertebral discs from 9-month-old mice stained with haematoxylin and eosin (H&E) and safranin O to detect proteoglycans. Arrows point to the annulus fibrosus. **k**, Representative images of gastrocnemius muscle sections from 8–11-month-old *Vav-iCre^{+/+};Ercc1^{fl/fl}* and littermate control mice after cardiotoxin injury (Methods) stained with haematoxylin and eosin or immunostained for M1 (CD68, green) and M2 (CD163, red) macrophages. **l**, Quantification of the ratio of M2/M1 macrophages ($n = 4$ *Vav-iCre^{+/+}*; $n = 8$ *Vav-iCre^{+/+};Ercc1^{fl/fl}* mice). **m**, Body weight and grip strength of *Vav-iCre^{+/+};Ercc1^{fl/fl}* and littermate controls at the indicated ages ($n = 8$ *Vav-iCre^{+/+};Ercc1^{fl/fl}*; $n = 4$ *Vav-iCre^{+/+}* at both ages). Data are mean \pm s.d. * $P < 0.05$, $\infty P < 0.01$, $\nabla P < 0.001$, # $P < 0.0001$, two-tailed unpaired Student's *t*-test (**a, b, d, e, h, i, l, m**) or two-way ANOVA with Tukey's test (**c**).

Article



Extended Data Fig. 7 | Age-associated increase in serum SASP factors of $Vav-iCre^{+/-};Ercc1^{-/-}$ mice and wild-type mice. a. This is an extension of the data shown in Fig. 3k, including two younger ages of mice. Circulating SASP factors were measured by ELISA ($n=3$ for 2–3-month-old, $n=4$ for 5-month-old, $n=5-7$ for 8–11-month-old, $n=7$ for 24-month-old) (see Supplementary Table 3 for sample size details). Data are mean \pm s.d. * $P < 0.05$, $\infty P < 0.01$, $\nabla P < 0.001$, # $P < 0.0001$, two-way ANOVA with Tukey's test. **b.** Haematoxylin and eosin

sections of brain, kidney and liver from 17-month-old $Vav-iCre^{+/-};Ercc1^{-/-}$ and littermate controls ($n=5$ mice per group) were scored for age-associated histopathological lesions using the Geropathology Grading Platform to generate a composite lesion score for each organ (CLS). Data are mean \pm s.d. P values (not significant) were determined by two-tailed unpaired Student's t -test.

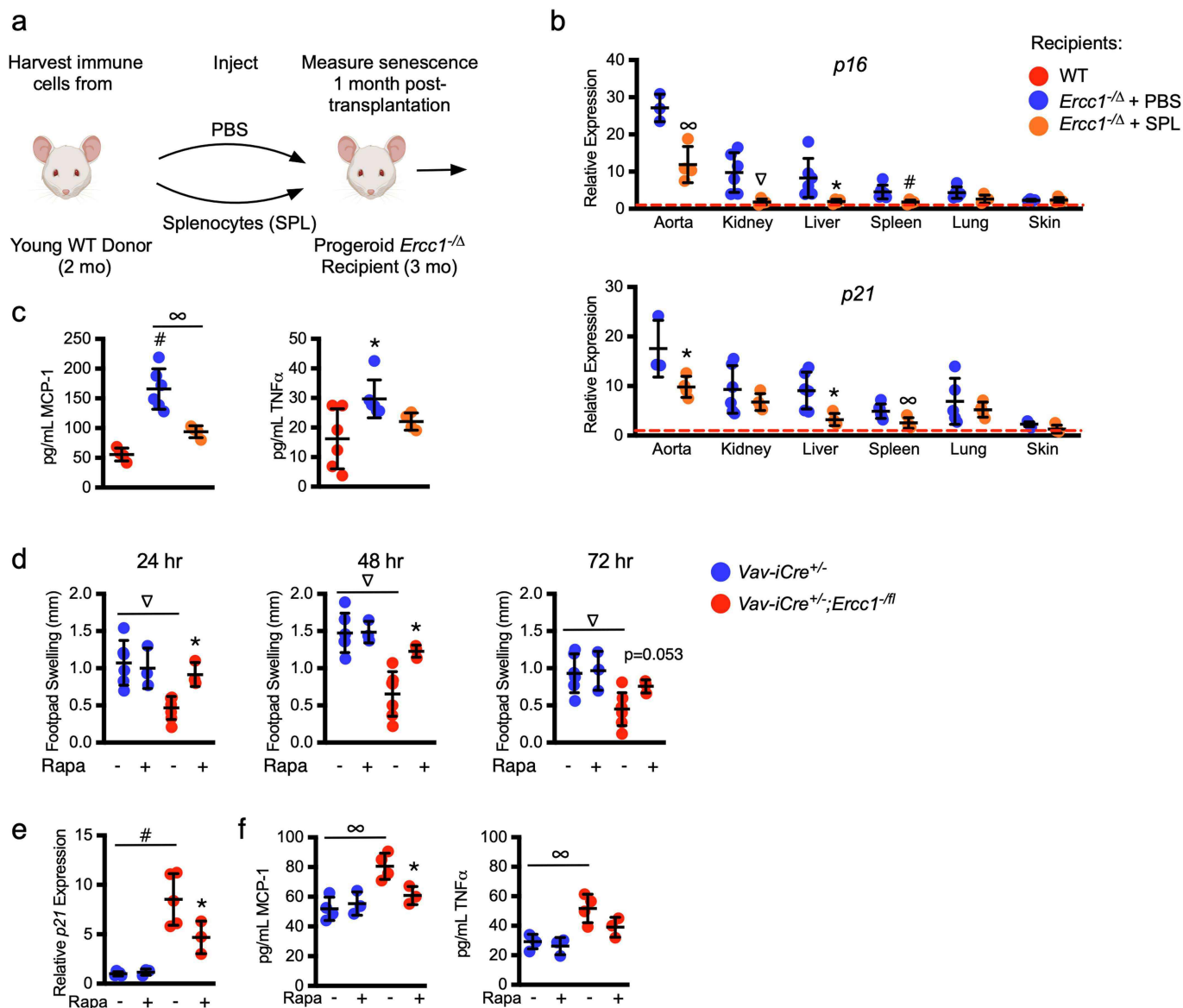
a**b****c**

Extended Data Fig. 8 | See next page for caption.

Article

Extended Data Fig. 8 | Time course of bioluminescence signal in p16-luciferase mice transplanted with splenocytes and tissue distribution of transplanted cells. **a**, Splenocytes from 8–10-month-old *Vav-iCre^{+/+};Ercc1^{-/-}*, *Vav-iCre^{+/+}* controls, or 2-year-old wild-type mice were injected retro-orbitally into 3–4-month-old *p16^{INK4+/Luc}* senescence reporter mice ($n = 2$ donor mice per genotype) as described in Fig. 4. Tissues were collected from recipient mice 2 weeks after the final imaging and the expression of *p21* was measured by qRT-PCR. Data are mean \pm s.d. * $P < 0.05$, $\infty P < 0.01$, one-way ANOVA with Tukey's test. **b**, Splenocytes (5×10^6 cells) from 9–10-month-old *Vav-iCre^{+/+};Ercc1^{-/-}* and *Vav-iCre^{+/+}* mice were injected retro-orbitally into 3–4-month-old *p16^{Luc/Luc}* senescence reporter mice ($n = 2$ donor mice per genotype; $n = 4$ *p16^{Luc/Luc}*

recipient mice for *Vav-iCre^{+/+};Ercc1^{-/-}* splenocytes; $n = 3$ receiving *Vav-iCre^{+/+}* splenocytes). Weekly measurements of luminescence in recipient reporter mice. Data are mean \pm s.d. * $P < 0.05$, $\infty P < 0.01$, two-tailed unpaired Student's *t*-test. **c**, Splenocytes from 7- or 26-month-old male mice were injected retro-orbitally into female mice to track distribution of the transplanted cells ($n = 2$ donor mice and $n = 3$ recipient mice per age group; $n = 2$ uninjected controls). Tissues were collected 24 h after injection. Expression of the Sry gene on the Y chromosome measured by qRT-PCR in RNA isolated from tissues of recipient mice was used to track homing of immune cells to various recipient mouse organs. There was little difference in immune cell homing if the donor mice were young or old.



Extended Data Fig. 9 | Suppression of senescence in progeroid mice by transplantation of young immune cells. **a**, Schematic of adoptive transfer: 3-month-old progeroid *Ercc1*^{-Δ/Δ} mice ($n=4$ mice/treatment group) were injected retro-orbitally with 5×10^6 splenocytes from 2-month-old WT mice or vehicle only (PBS) ($n=6$ donors). One month later, the recipient mice and uninjected age-matched wild-type mice were euthanized, and tissues collected. **b**, Expression of senescence markers in organs of recipient mice ($n=4$ *Ercc1*^{-Δ/Δ} + splenocytes; $n=3-6$ *Ercc1*^{-Δ/Δ} + PBS) (see Supplementary Table 3 for sample size details by organ/endpoint). Gene expression was normalized to that of uninjected, age-matched wild-type controls ($n=4-7$) represented as horizontal dashed line. **c**, SASP factor proteins MCP-1 and TNF were measured

in the serum of recipient mice by multiplex ELISA ($n=4$ *Ercc1*^{-Δ/Δ} + splenocytes; $n=6$ *Ercc1*^{-Δ/Δ} + PBS) and compared to untreated, age-matched wild-type mice ($n=4-6$). **d**, Footpad swelling of mice describe above and in Fig. 5f at several time points after antigenic challenge ($n=3/7$ *Vav-iCre*^{+/-};*Ercc1*^{-Δ/Δ} or $n=3/6$ *Vav-iCre*^{+/-} mice +/- rapamycin, respectively). **e**, Expression of *p21* in PBMCs, measured by qRT-PCR. **f**, Serum MCP-1 and TNF measured by multiplex ELISA ($n=3/5$ +/- rapamycin, respectively). Data are mean \pm s.d. * $P < 0.05$, $\infty P < 0.01$, $\nabla P < 0.001$, # $P < 0.0001$ one-way ANOVA (**b, c**) or two-way ANOVA (**d-f**) with Tukey's test. Mouse images in schematic were used with permission from BioRender.

Article

Extended Data Table 1 | Complete blood counts with differential

| | WBC | Lym | Mono | Gran | RBC | HGB | HCT | PLT | |
|-------------------------------------------------------------|--------------------|--------------------|--------------------|--------------------|--------------------|------------|------------|--------------------|---|
| | $10^3/\text{mm}^2$ | $10^3/\text{mm}^2$ | $10^3/\text{mm}^2$ | $10^3/\text{mm}^2$ | $10^4/\text{mm}^2$ | g/dL | % | $10^3/\text{mm}^2$ | n |
| 3 months | | | | | | | | | |
| <i>Vav-iCre</i> ^{-/-} | 9.2 ± 1.6 | 6.8 ± 1.1 | 0.6 ± 0.1 | 1.9 ± 0.7 | 9.4 ± 1.3 | 13.4 ± 1.0 | 41.6 ± 2.3 | 714 ± 123 | 4 |
| <i>VavCre</i> ^{-/-} ; <i>Ercc1</i> ^{-/-β} | 10.1 ± 1.1 | 8.2 ± 1.3 | 0.4 ± 0.2 | 1.4 ± 0.4 | 9.8 ± 0.7 | 14.6 ± 0.6 | 41.7 ± 2.8 | 848 ± 123 | 3 |
| 5-6 months | | | | | | | | | |
| <i>Vav-iCre</i> ^{-/-} | 8.8 ± 1.0 | 6.8 ± 0.8 | 0.6 ± 0.2 | 1.4 ± 0.3 | 9.7 ± 0.7 | 14.1 ± 1.6 | 39.7 ± 3.6 | 618 ± 140 | 7 |
| <i>VavCre</i> ^{-/-} ; <i>Ercc1</i> ^{-/-β} | 5.2 ± 0.6** | 2.8 ± 0.6**** | 0.7 ± 0.2 | 1.7 ± 0.4 | 9.3 ± 1.0 | 14.0 ± 1.0 | 40.8 ± 2.5 | 633 ± 153 | 6 |
| 12 months | | | | | | | | | |
| <i>Vav-iCre</i> ^{-/-} | 8.6 ± 2.6 | 6.5 ± 1.8 | 0.5 ± 0.2 | 1.6 ± 0.7 | 9.8 ± 0.8 | 14.0 ± 1.5 | 41.3 ± 1.6 | 554 ± 233 | 8 |
| <i>VavCre</i> ^{-/-} ; <i>Ercc1</i> ^{-/-β} | 2.5 ± 1.3**** | 1.0 ± .5**** | 0.3 ± 0.1 | 1.0 ± 0.3 | 9.2 ± 0.7 | 14.0 ± 1.1 | 40.6 ± 2.5 | 504 ± 166 | 8 |
| 16-18 months | | | | | | | | | |
| <i>Vav-iCre</i> ^{-/-} | 6.7 ± 2.2 | 4.7 ± 1.5 | 0.5 ± 0.1 | 1.0 ± 0.2 | 9.6 ± 0.8 | 14.5 ± 1.6 | 40.2 ± 5.0 | 490 ± 160 | 5 |
| <i>VavCre</i> ^{-/-} ; <i>Ercc1</i> ^{-/-β} | 2.0 ± 1.0*** | 0.9 ± 0.6*** | 0.3 ± 0.2 | 0.8 ± 0.3 | 8.7 ± 0.9 | 13.2 ± 1.4 | 37.3 ± 4.2 | 510 ± 107 | 6 |

Data are mean ± s.d. Statistical significance was determined using a two-tailed unpaired Student's t-test. ***P* < 0.01, ****P* < 0.001, *****P* < 0.0001.

Reporting Summary

Nature Research wishes to improve the reproducibility of the work that we publish. This form provides structure for consistency and transparency in reporting. For further information on Nature Research policies, see [Authors & Referees](#) and the [Editorial Policy Checklist](#).

Statistics

For all statistical analyses, confirm that the following items are present in the figure legend, table legend, main text, or Methods section.

n/a Confirmed

- The exact sample size (n) for each experimental group/condition, given as a discrete number and unit of measurement
- A statement on whether measurements were taken from distinct samples or whether the same sample was measured repeatedly
- The statistical test(s) used AND whether they are one- or two-sided
Only common tests should be described solely by name; describe more complex techniques in the Methods section.
- A description of all covariates tested
- A description of any assumptions or corrections, such as tests of normality and adjustment for multiple comparisons
- A full description of the statistical parameters including central tendency (e.g. means) or other basic estimates (e.g. regression coefficient) AND variation (e.g. standard deviation) or associated estimates of uncertainty (e.g. confidence intervals)
- For null hypothesis testing, the test statistic (e.g. F , t , r) with confidence intervals, effect sizes, degrees of freedom and P value noted
Give P values as exact values whenever suitable.
- For Bayesian analysis, information on the choice of priors and Markov chain Monte Carlo settings
- For hierarchical and complex designs, identification of the appropriate level for tests and full reporting of outcomes
- Estimates of effect sizes (e.g. Cohen's d , Pearson's r), indicating how they were calculated

Our web collection on [statistics for biologists](#) contains articles on many of the points above.

Software and code

Policy information about [availability of computer code](#)

Data collection

FlowJo 9.0 was used to collect flow cytometric and CyTOF data. Cytobank was used for VisNE analysis.

Data analysis

Prism 8.0 was used for all statistical assessments.

For manuscripts utilizing custom algorithms or software that are central to the research but not yet described in published literature, software must be made available to editors/reviewers. We strongly encourage code deposition in a community repository (e.g. GitHub). See the Nature Research [guidelines for submitting code & software](#) for further information.

Data

Policy information about [availability of data](#)

All manuscripts must include a [data availability statement](#). This statement should provide the following information, where applicable:

- Accession codes, unique identifiers, or web links for publicly available datasets
- A list of figures that have associated raw data
- A description of any restrictions on data availability

The datasets generated during and/or analysed during the current study are available from the corresponding author on reasonable request.

Field-specific reporting

Please select the one below that is the best fit for your research. If you are not sure, read the appropriate sections before making your selection.

- Life sciences Behavioural & social sciences Ecological, evolutionary & environmental sciences

For a reference copy of the document with all sections, see [nature.com/documents/nr-reporting-summary-flat.pdf](https://www.nature.com/documents/nr-reporting-summary-flat.pdf)

Life sciences study design

All studies must disclose on these points even when the disclosure is negative.

| | |
|-----------------|-----------------------------------------------------------------------------------------------------------------------------------------------------|
| Sample size | We note that no power calculations were used. Sample sizes are based on previously published experiments where differences were observed. |
| Data exclusions | No samples were excluded from data analysis. |
| Replication | Results shown are representative of several independently performed experiments. Number of biological replicates is as described in figure legends. |
| Randomization | Treatment groups were randomly assigned to mice. |
| Blinding | Investigators were blinded to the allocation during experiments and outcomes assessments. |

Reporting for specific materials, systems and methods

We require information from authors about some types of materials, experimental systems and methods used in many studies. Here, indicate whether each material, system or method listed is relevant to your study. If you are not sure if a list item applies to your research, read the appropriate section before selecting a response.

Materials & experimental systems

| n/a | Included in the study |
|-------------------------------------|-----------------------------------------------------------------|
| <input type="checkbox"/> | <input checked="" type="checkbox"/> Antibodies |
| <input type="checkbox"/> | <input checked="" type="checkbox"/> Eukaryotic cell lines |
| <input checked="" type="checkbox"/> | <input type="checkbox"/> Palaeontology |
| <input type="checkbox"/> | <input checked="" type="checkbox"/> Animals and other organisms |
| <input checked="" type="checkbox"/> | <input type="checkbox"/> Human research participants |
| <input checked="" type="checkbox"/> | <input type="checkbox"/> Clinical data |

Methods

| n/a | Included in the study |
|-------------------------------------|----------------------------------------------------|
| <input checked="" type="checkbox"/> | <input type="checkbox"/> ChIP-seq |
| <input type="checkbox"/> | <input checked="" type="checkbox"/> Flow cytometry |
| <input checked="" type="checkbox"/> | <input type="checkbox"/> MRI-based neuroimaging |

Antibodies

Antibodies used

WB: anti-ERCC1 (Santa Cruz Biotechnology, catalog #sc-17089, 1:400)
 WB: anti-γH2AX (Novus Biologicals, catalog# NB100-384, 1:2000)
 WB: anti-GAPDH (Abcam, catalog# ab8425, 1:5000)
 WB: anti-mouse HRP (Cell Signaling Technology, catalog #7076S, 1:2000)
 WB: anti-rabbit HRP secondary antibody (Thermo-Fisher, catalog # 656120, 1:2000)
 IF: anti-Albumin (Abcam, catalog# ab207327, 1:500)
 IF: anti-CD68 (Abcam, catalog# ab53444, 1:200)
 IF: anti-CD163 (Santa Cruz Biotechnology, catalog# sc-33560, 1:50)
 IF: anti-rabbit Alexafluor 594-conjugated (Invitrogen, catalog# A21207, 1:500)
 IF: anti-rat Alexafluor 488-conjugated (Invitrogen, catalog# A21208, 1:500)
 IF: anti-Aggregan (Millipore, catalog# ab10331, 1:400)
 IF: anti-KSP-Cadherin (Novus Biologicals, catalog # NBP2-53221, 1:100)
 FACS: anti-CD16/CD32 mAb (BD, catalog# 553141, 1:600)
 FACS: anti-CD3-PE (BD, catalog# 553063, clone 145-2C11, 1:200)
 FACS: anti-NK1.1-FITC (BD, catalog# 553164, clone PK136, 1:400)
 FACS: anti-CD19-APC (eBioscience, catalog# 17-0193-82, clone 1D3,)
 FACS: anti-B220-FITC (eBioscience, catalog# 11-0452-82, clone RA3-682, 1:200)
 FACS: anti-F4/80-PE-Cy7 (eBioscience, catalog# 25-4801-82, clone BM8, 1:100)
 FACS: anti-Cd11b-PE (BD, catalog# 557397, clone M1/70, 1:100)
 ACS: anti-Gr-1-PE (eBioscience, catalog# 12-5931-82, clone RB6-8C50, 1:800)
 FACS: anti-CD43-PE (eBioscience, catalog# 12-0431-82, clone eBioR2/60, 1:600)
 FACS: anti-CD11c-eFluor450 (eBioscience, catalog# 48-0114-82, clone N4180, 1:400)
 FACS: anti-IgM-eFluor450 (eBioscience, catalog# 48-5890-82, clone eB121-15F9, 1:600)
 FACS: anti-CD8a-eFluor450 (eBioscience, catalog# 48-0081-82, clone 63-6.79, 1:800)
 FACS: anti-Ly-6C-eFluor450 (eBioscience, catalog# 48-5932-82, clone HK1.4, 1:800)
 FACS: anti-CD4-PerCP (BD, catalog# 553052, clone RM4-5, 1:300)
 FACS: anti-CD44-PE (BD, catalog# 561860, clone IM7, 1:1500)
 FACS: anti-PD-1-APC (BD, catalog# 562671, clone J43, 1:600)
 FACS: anti-CD127-PE-Cy7 (BD, catalog# 560733, SB/199, 1:1500)
 CyTOF: Anti-CD45-089Y (Fluidigm, clone 30-F11, 1:200)
 CyTOF: Anti-CD39-a4aPr (Biolegend, clone 24DMS, 1:100)
 CyTOF: Anti-Eomes-142Nd (ThermoFisher, clone Dan11mag, 1:100)
 CyTOF: Anti-TCRb-143Nd (Fluidigm, clone H57-597, 1:400)

CyTOF: Anti-CD11b-171Yb (Biolegend, clone M1/70, 1:400)
 CyTOF: Anti-Fas-172Yb (Biolegend, clone SA367H8, 1:100)
 CyTOF: Anti-p16-173Yb (Proteintech, 10883-1-AP, 1:100)
 CyTOF: Anti-CD223 (LAG-3)-174Yb (Biolegend, C9B7W, 1:100)
 CyTOF: Anti-iNOS (NOS2)-175Lu (Thermo-Fisher, clone CXNFT, 1:100)
 CyTOF: Anti-CD44-176Yb (Biolegend, clone IM7, 1:100)
 CyTOF: Anti-CD11c-209Bi (Fluidigm, clone N418, 1:100)
 CyTOF: Anti-BATF-154Sm (Fluidigm, clone D7C5, 1:200)
 CyTOF: Anti-Tbet-155Gd (Biolegend, clone 4B10, 1:100)
 CyTOF: Anti-CD90.2/Thy-1.2-156Gd (Fluidigm, clone 30-H12, 1:400)
 CyTOF: Anti-FoxP3-158Gd (Fluidigm, clone FJK-16s, 1:100)
 CyTOF: Anti-CD279 (PD-1)-159Tb (Fluidigm, clone RMP1-30, 1:100)
 CyTOF: Anti-CD62L-160Gd (Fluidigm, clone MEL14, 1:100)
 CyTOF: Anti-Ki-67-161Dy (Fluidigm, clone B56, 1:100)
 CyTOF: Anti-p21-162Dy (SCBT, clone F5, 1:100)
 CyTOF: Anti-CD4-163Dy (Biolegend, clone RM4-5, 1:200)
 CyTOF: Anti-CD73-164Dy (Biolegend, clone TY/11.8, 1:100)
 CyTOF: Anti-Thy1.1-165Ho (Biolegend, clone OX-7, 1:200)
 CyTOF: Anti-CD19-166Er (Fluidigm, clone 6D5, 1:200)
 CyTOF: Anti-CD38-167Er (Fluidigm, clone 90, 1:100)
 CyTOF: Anti-CD8a-168Er (Fluidigm, clone 53-6.7, 1:400)
 CyTOF: Anti-Cd272 (BTLA)-169Tm (Thermo-Fisher, clone 6F7, 1:100)
 CyTOF: Anti-CD161 (NK1.1)-170Erc (Fluidigm, clone PK136, 1:200)
 CyTOF: Anti-Tcf1-144Nd (R&D Systems, clone 812145, 1:200)
 CyTOF: Anti-CD69-145Nd (Fluidigm, clone H1.2F3, 1:200)
 CyTOF: Anti-GATA3-146Nd (Fluidigm, clone TWAJ, 1:100)
 CyTOF: Anti-CENP-B-147Sm (Abcam, ab25734, 1:100)
 CyTOF: Anti-ROR-gamma-148Nd (Abcam, B2D, 1:100)
 CyTOF: Anti-CD366 (Tim-3)-149Sm (Biolegend, clone RMT3-23, 1:100)
 CyTOF: Anti-IRF4-150Nd (Biolegend, clone IRF4.3E4, 1:100)
 CyTOF: Anti-CD25 (IL-2R)-151Eu (Fluidigm, clone 3C7, 1:100)
 CyTOF: Anti-CD3e-152Sm (Fluidigm, clone 145-2C11, 1:400)
 CyTOF: Anti-CD28-153Eu (Biolegend, clone 37.51, 1:100)

Validation

All antibodies are from commercially available sources and have been validated from the manufacturer with supporting publications found on the manufacturer's website. See below for summary:

CyTOF
 Anti-CD45-089Y (Fluidigm, clone 30-F11, 1:200)
 Species: Mouse
 Application: CyTOF

CyTOF
 Anti-CD39-141Pr (Biolegend, clone 24DMS, 1:100)
 Species: Mouse
 Application: CyTOF

CyTOF
 Anti-Eomes-142Nd (Thermo-Fisher, clone Dan11mag, 1:100)
 Species: Mouse
 Application: CyTOF

CyTOF
 Anti-TCRb-143Nd (Fluidigm, clone H57-597, 1:400)
 Species: Mouse
 Application: CyTOF

CyTOF
 Anti-Tcf1-144Nd (R&D Ststens, clone 812145, 1:200)
 Species: Mouse
 Application: CyTOF

CyTOF
 Anti-CD69-145Nd (Fluidigm, clone H1.2F3, 1:200)
 Species: Mouse
 Application: CyTOF

CyTOF
 Anti-GATA3-146Nd (Fluidigm, clone TWAJ, 1:100)
 Species: Mouse
 Application: CyTOF

CyTOF

Anti-CENP-B-147Sm (Abcam, ab25734, 1:100)

Species: Mouse

Application: CyTOF

CyTOF

Anti-ROR-gamma-148Nd (Abcam, B2D, 1:100)

Species: Mouse

Application: CyTOF

CyTOF

Anti-CD366 (Tim-3)-149Sm (Biolegend, clone RMT3-23, 1:100)

Species: Mouse

Application: CyTOF

CyTOF

Anti-IRF4-150Nd (Biolegend, clone IRF4.3E4, 1:100)

Species: Mouse

Application: CyTOF

CyTOF

Anti-CD25 (IL-2R)-151Eu (Fluidigm, clone 3C7, 1:100)

Species: Mouse

Application: CyTOF

CyTOF

Anti-CD3e-152Sm (Fluidigm, clone 145-2C11, 1:400)

Species: Mouse

Application: CyTOF

CyTOF

Anti-CD28-153Eu (Biolegend, clone 37.51, 1:100)

Species: Mouse

Application: CyTOF

CyTOF

Anti-BATF-154Sm (Fluidigm, clone D7C5, 1:200)

Species: Mouse

Application: CyTOF

CyTOF

Anti-Tbet-155Gd (Biolegend, clone 4B10, 1:100)

Species: Mouse

Application: CyTOF

CyTOF

Anti-CD90.2/Thy-1.2-156Gd (Fluidigm, clone 30-H12, 1:400)

Species: Mouse

Application: CyTOF

CyTOF

Anti-FoxP3-158Gd (Fluidigm, clone FJK-16s, 1:100)

Species: Mouse

Application: CyTOF

CyTOF

Anti-CD279 (PD-1)-159Tb (Fluidigm, clone RMP1-30, 1:100)

Species: Mouse

Application: CyTOF

CyTOF

Anti-CD62L-160Gd (Fluidigm, clone MEL14, 1:100)

Species: Mouse

Application: CyTOF

CyTOF

Anti-Ki-67-161Dy (Fluidigm, clone B56, 1:100)

Species: Mouse

Application: CyTOF

CyTOF

Anti-p21-162Dy (SCBT, clone F5, 1:100)

Species: Mouse

Application: CyTOF

CyTOF
Anti-CD4-163Dy (Biolegend, clone RM4-5, 1:200)
Species: Mouse
Application: CyTOF

CyTOF
Anti-CD73-164Dy (Biolegend, clone TY/11.8, 1:100)
Species: Mouse
Application: CyTOF

CyTOF
Anti-Thy1.1-165Ho (Biolegend, clone OX-7, 1:200)
Species: Mouse
Application: CyTOF

CyTOF
Anti-CD19-166Er (Fluidigm, clone 6D5, 1:200)
Species: Mouse
Application: CyTOF

CyTOF
Anti-CD38-167Er (Biolegend, clone 90, 1:100)
Species: Mouse
Application: CyTOF

CyTOF
Anti-CD8a-168Er (Fluidigm, clone 53-6.7, 1:400)
Species: Mouse
Application: CyTOF

CyTOF
Anti-CD272 (BTLA)-169Tm (Thermo-Fisher, clone 6F7, 1:100)
Species: Mouse
Application: CyTOF

CyTOF
Anti-CD161 (NK1.1)-170Er (Fluidigm, clone PK136, 1:200)
Species: Mouse
Application: CyTOF

CyTOF
Anti-CD11b-171Yb (Biolegend, clone M1/70, 1:400)
Species: Mouse
Application: CyTOF

CyTOF
Anti-Fas-172Yb (Biolegend, clone SA367H8, 1:100)
Species: Mouse
Application: CyTOF

CyTOF
Anti-p16-173Yb (Proteintech, 10883-1-AP, 1:100)
Species: Mouse
Application: CyTOF

CyTOF
Anti-CD223 (LAG-3)-174Yb (Biolegend, clone C9B7W, 1:100)
Species: Mouse
Application: CyTOF

CyTOF
Anti-iNOS (NOS2)-175Lu (Thermo-Fisher, clone CXNFT, 1:100)
Species: Mouse
Application: CyTOF

CyTOF
Anti-CD44-176Yb (Biolegend, clone IM7, 1:100)
Species: Mouse
Application: CyTOF

CyTOF
Anti-CD11c-209Bi (Fluidigm, clone N418, 1:100)
Species: Mouse
Application: CyTOF

WB
anti-ERCC1 (Santa Cruz Biotechnology, catalog #sc-17809, 1:400)
Species: mouse, rat, and human
Applications: WB, IP, IF, IHC, ELISA

WB
anti-γH2AX (Novus Biologicals, catalog# NB100-384, 1:2000)
Species: canine, mouse, rat, and human
Applications: WB, IP, IF, IHC, ELISA, FACS

WB:
anti-alpha-Tubulin (Abcam, catalog# ab4074, 1:5000)
Species: canine, chicken, cow, mouse, rat, and human
Applications: WB, IF, IHC

IF
anti-Albumin (Abcam, catalog# ab207327, 1:500)
Species: mouse, rat, and human
Applications: WB, IP, IF, IHC, FACS

IF
anti-CD68 (Abcam, catalog# ab53444, 1:200)
Species: mouse
Applications: WB, IP, IF, IHC, ELISA, FACS

IF
anti-CD163 (Santa Cruz Biotechnology, catalog# sc-33560, 1:50)
Species: mouse, rat, and human
Applications: WB, IP, IF, IHC, FACS

IF
anti-Aggrecan (Millipore, catalog# ab1031, 1:400)
Species: mouse
Applications: WB, IP, IF, IHC

IF
anti-rabbit Alexafluor 594-conjugated (Invitrogen, catalog# A21207, 1:500)
Species: N/A
Applications: IF, IHC, FACS

IF
anti-rat Alexafluor 488-conjugated (Invitrogen, catalog# A21208, 1:500)
Species: N/A
Applications: IF, IHC, FACS

IF
anti-KSP-Cadherin (Novus Biologicals, catalog # NBP2-53221, 1:100)
Species: Rabbit
Applications: IF

FACS
anti-CD16/CD32 mAb (BD, catalog# 553141, 1:600)
Species: mouse
Applications: FACS

FACS
anti-CD3-PE (BD, catalog# 553063, clone 145-2C11, 1:200)
Species: mouse
Applications: FACS

FACS
anti-NK1.1-FITC (BD, catalog# 553164, clone PK136, 1:400)
Species: mouse
Applications: FACS

FACS
anti-CD19-APC (eBioscience, catalog# 17-0193-82, clone 1D3, 1:800)
Species: mouse
Applications: FACS

FACS
anti-B220-FITC (eBioscience, catalog# 11-0452-82, clone RA3-682, 1:200)
Species: mouse
Applications: FACS

FACS
anti-F4/80-PE-Cy7 (eBioscience, catalog# 25-4801-82, clone BM8, 1:800)
Species: mouse
Applications: FACS

FACS
anti-Cd11b-PE (BD, catalog# 557397, clone M1/70, 1:100)
Species: mouse
Applications: FACS

FACS
anti-Gr-1-PE (eBioscience, catalog# 12-5931-82, clone RB6-8C50, 1:800)
Species: mouse
Applications: FACS

FACS
anti-CD43-PE (eBioscience, catalog# 12-0431-82, clone eBioR2/60, 1:600)
Species: mouse
Applications: FACS

FACS
anti-CD11c-eFluor450 (eBioscience, catalog# 48-0114-82, clone N4180, 1:400)
Species: mouse
Applications: FACS

FACS
anti-IgM-eFluor450 (eBioscience, catalog# 48-5890-82, clone eB121-15F9, 1:600)
Species: mouse
Applications: FACS

FACS
anti-CD8a-eFluor450 (eBioscience, catalog# 48-0081-82, clone 63-6.79, 1:800)
Species: mouse
Applications: FACS

FACS
anti-Ly-6C-eFluor450 (eBioscience, catalog# 48-5932-82, clone HK1.4, 1:800)
Species: mouse
Applications: FACS

FACS
anti-CD4-PerCP (BD, catalog# 553052, clone RM4-5, 1:300)
Species: mouse
Applications: FACS

FACS
anti-CD44-PE (BD, catalog# 561860, clone IM7, 1:1500)
Species: mouse
Applications: FACS

FACS
anti-PD-1-APC (BD, catalog# 562671, clone J43, 1:600)
Species: mouse
Applications: FACS

FACS
anti-CD127-PE-Cy7 (BD, catalog# 560733, SB/199, 1:1500)
Species: mouse
Applications: FACS

Eukaryotic cell lines

Policy information about [cell lines](#)

| | |
|----------------------------------------------------------------------|-----------------------------------------------------------------------------------------|
| Cell line source(s) | K562 (ATCC) |
| Authentication | Cells were purchased and used directly from ATCC |
| Mycoplasma contamination | Cells were tested for mycoplasma contamination and found to be negative for mycoplasma. |
| Commonly misidentified lines (See ICLAC register) | N/A |

Animals and other organisms

Policy information about [studies involving animals](#); [ARRIVE guidelines](#) recommended for reporting animal research

| | |
|-------------------------|-----------------------------------------------------------------------------------------------------------------------------------------------------------------------------------------------------------------------------------------------------------------------------------------|
| Laboratory animals | All animals used for experiments (WT, p16-luciferase, Ercc1- Δ , Ercc1-/c, Vav-iCre+/-, Vav-iCre+/-,Ercc1-/fl) were C57BL/6J:FVB/N F1 hybrid mice. Mice were used at multiple age points (as described in the manuscript) and both male and female mice were used in this study. |
| Wild animals | No wild animals were used in this study. |
| Field-collected samples | No field-collected samples were used in this study. |
| Ethics oversight | All studies were approved by the Institutional Biosafety Committee and Institutional Animal Care and Use Committee at The Scripps Research Institute and the University of Minnesota |

Note that full information on the approval of the study protocol must also be provided in the manuscript.

Flow Cytometry

Plots

Confirm that:

- The axis labels state the marker and fluorochrome used (e.g. CD4-FITC).
- The axis scales are clearly visible. Include numbers along axes only for bottom left plot of group (a 'group' is an analysis of identical markers).
- All plots are contour plots with outliers or pseudocolor plots.
- A numerical value for number of cells or percentage (with statistics) is provided.

Methodology

| | |
|---------------------------|-------------------------------------------------------------------------------------------------------------------------------------|
| Sample preparation | All information is as described in the methods section |
| Instrument | Helios (Fluidigm), Aria III, FACS Canto II and LSR II (BD Bioscience) |
| Software | FACSDiva 8.0.1 |
| Cell population abundance | For sorting experiments, 5×10^4 of each cell population was sorted from each mouse for use in gene expression experiments. |
| Gating strategy | This information can be found in Extended Data Fig. 5 and 9. Additional information can be provided if necessary. |

Tick this box to confirm that a figure exemplifying the gating strategy is provided in the Supplementary Information.